

1 **Potent human neutralizing antibodies elicited by SARS-CoV-2 infection**

2 Bin Ju^{1,2,*}, Qi Zhang^{3,*}, Xiangyang Ge¹, Ruko Wang³, Jiazen Yu¹, Sisi Shan³,
3 Bing Zhou¹, Shuo Song¹, Xian Tang¹, Jinfang Yu⁴, Jiwan Ge⁴, Jun Lan⁴, Jing
4 Yuan⁵, Haiyan Wang¹, Juanjuan Zhao^{1,2}, Shuye Zhang⁶, Youchun Wang⁷,
5 Xuanling Shi³, Lei Liu^{1,2}, Xinquan Wang⁴, Zheng Zhang^{1,2#}, and Linqi Zhang^{3#}

6

7 ¹Institute for Hepatology, National Clinical Research Center for Infectious
8 Disease, Shenzhen Third People's Hospital, Shenzhen 518112, Guangdong
9 Province, China

10 ²The Second Affiliated Hospital, School of Medicine, Southern University of
11 Science and Technology, Shenzhen 518055, Guangdong Province, China.

12 ³Center for Global Health and Infectious Diseases, Comprehensive AIDS
13 Research Center, and Beijing Advanced Innovation Center for Structural
14 Biology, School of Medicine, Tsinghua University, Beijing 100084, China

15 ⁴The Ministry of Education Key Laboratory of Protein Science, Beijing
16 Advanced Innovation Center for Structural Biology, Beijing Frontier Research
17 Center for Biological Structure, Collaborative Innovation Center for Biotherapy,
18 School of Life Sciences, Tsinghua University, 100084 Beijing, China

19 ⁵Department for Infectious Diseases, Shenzhen Third People's Hospital,
20 Shenzhen, Guangdong Province 518112, China

21 ⁶Shanghai Public Health Clinical Center and Institute of Biomedical Sciences,
22 Fudan University, Shanghai 201508, China

23 ⁷Division of HIV/AIDS and Sex-Transmitted Virus Vaccines, National Institutes
24 for Food and Drug Control, Beijing, China.

25 *These authors contributed equally to this work.

26 #Correspondence: zhangzheng1975@aliyun.com (Z.Z) or
27 zhanglinqi@tsinghua.edu.cn (L.Z.)

28

29

30 **Abstract**

31 The pandemic caused by emerging coronavirus SARS-CoV-2 presents a
32 serious global public health emergency in urgent need of prophylactic and
33 therapeutic interventions. SARS-CoV-2 cellular entry depends on binding
34 between the viral Spike protein receptor-binding domain (RBD) and the
35 angiotensin converting enzyme 2 (ACE2) target cell receptor. Here, we report
36 on the isolation and characterization of 206 RBD-specific monoclonal
37 antibodies (mAbs) derived from single B cells of eight SARS-CoV-2 infected
38 individuals. These mAbs come from diverse families of antibody heavy and light
39 chains without apparent enrichment for particular families in the repertoire. In
40 samples from one patient selected for further analyses, we found coexistence
41 of germline and germline divergent clones. Both clone types demonstrated
42 impressive binding and neutralizing activity against pseudovirus and live SARS-
43 CoV-2. However, the antibody neutralizing potency is determined by
44 competition with ACE2 receptor for RBD binding. Surprisingly, none of the
45 SARS-CoV-2 antibodies nor the infected plasma cross-reacted with RBDs from
46 either SARS-CoV or MERS-CoV although substantial plasma cross-reactivity
47 to the trimeric Spike proteins from SARS-CoV and MERS-CoV was found.
48 These results suggest that antibody response to RBDs is viral species-specific
49 while that cross-recognition target regions outside the RBD. The specificity and
50 neutralizing characteristics of this plasma cross-reactivity requires further
51 investigation. Nevertheless, the diverse and potent neutralizing antibodies
52 identified here are promising candidates for prophylactic and therapeutic
53 SARS-CoV-2 interventions.

54

55 **Introduction**

56 The source of the recent Coronavirus Disease 2019 (COVID-19) outbreak in
57 Wuhan, China is a novel pathogenic coronavirus, SARS-CoV-2 ¹⁻⁴. Its unique
58 pathogenesis and rapid international transmission poses a serious global
59 health emergency ⁵⁻⁹. SARS-CoV-2 belongs to the betacoronavirus family and
60 shares substantial genetic and functional similarity with other pathogenic
61 human betacoronaviruses, including Severe Acute Respiratory Syndrome
62 Coronavirus (SARS-CoV) and Middle East Respiratory Syndrome Coronavirus
63 (MERS-CoV) ^{2-4,10,11}. The virus is believed to have originated in bats, although
64 the source and animal reservoirs of SARS-CoV-2 remain uncertain ^{2-4,10-12}. No
65 SARS-CoV-2-specific treatments or vaccine are currently available but several
66 antiviral drugs including remdesivir are being investigated clinically.

67 SARS-CoV-2 utilizes an envelope homotrimeric Spike glycoprotein (S) to
68 interact with cellular receptor ACE2 ^{2,13,14}. Binding with ACE2 triggers a
69 cascade of cell membrane fusion events for viral entry. Each S protomer
70 consists of two subunits: a globular S1 domain at the N-terminal region, and the
71 membrane-proximal S2 and transmembrane domains. Determinants of host
72 range and cellular tropism are found in the RBD within the S1 domain, while
73 mediators of membrane fusion have been identified within the S2 domain ^{15,16}.
74 We and others have recently determined the high-resolution structure of SARS-
75 CoV-2 RBD bound to the N-terminal peptidase domain of ACE2 ^{14,17}. The
76 overall ACE2-binding mechanism is virtually the same between SARS-CoV-2
77 and SARS-CoV RBDs, indicating convergent ACE2-binding evolution between
78 these two viruses ¹⁸⁻²². This suggests that disruption of the RBD and ACE2
79 interaction would block SARS-CoV-2 entry into the target cell. Indeed, a few
80 such disruptive agents targeted to ACE2 have been shown to inhibit SARS-
81 CoV infection ^{23,24}. However, given the important physiological roles of ACE2 *in*
82 *vivo* ²⁵, these agents may have undesired side effects. Anti-RBD antibodies, on
83 the other hand, are therefore more favorable. Furthermore, SARS-CoV or
84 MERS-CoV RBD-based vaccine studies in experimental animals have also
85 shown strong polyclonal antibody responses that inhibit viral entry ^{15,26}. Such
86 critical proof-of-concept findings indicate that anti-RBD antibodies should be

87 able to effectively block SARS-CoV-2 entry. Here, we report on the isolation
88 and characterization of 206 RBD-specific mAbs derived from single B cells of
89 eight SARS-CoV-2 infected individuals. Using bioinformatic and biologic
90 characterization, we identified several mAbs with potent neutralizing activity
91 against pseudovirus and live SARS-CoV-2. However, no cross-reactivity between
92 RBDs from SARS-CoV or MERS-CoV was found, suggesting that the RBD-
93 based antibody response is viral species-specific. The potent neutralizing
94 antibodies identified here are promising candidates for prophylactic and
95 therapeutic SARS-CoV-2 interventions.

96 **Results**

97 **Plasma and B cell responses specific to SARS-CoV-2.** We collected
98 cross-sectional and longitudinal blood samples from eight
99 SARS-CoV-2-infected subjects during the early outbreak in Shenzhen (Table
100 S1). Samples were named by patient number and either A, B, or C depending
101 on collection sequence. Six patients (P#1 through P#4, P#8, and P#16) had
102 Wuhan travel history and the remaining two (P#5 and P#22) had direct contact
103 with those from Wuhan. P#1 through P#5 is a family cluster with the first
104 documented case of human-to-human transmission of SARS-CoV-2 in
105 Shenzhen ⁵. All subjects recovered and were discharged from the hospital
106 except for P#1 who succumbed to disease despite intensive intervention. To
107 analyze antibody binding, serial plasma dilutions were applied to enzyme-linked
108 immunosorbent assay (ELISA) plates coated with either recombinant RBD or
109 trimeric Spike derived from SARS-CoV-2, SARS-CoV, and MERS-CoV or
110 recombinant NP from SARS-CoV-2. Binding activity was visualized using
111 anti-human IgG secondary antibodies at an optical density (OD) of 450nm.
112 Varying degrees of binding were found across individuals and among samples
113 from the same individual. Samples from P#1, P#2, P#5, and P#16
114 demonstrated higher binding to both SARS-CoV-2 RBD and NP than the rest
115 (Figure 1A). Three sequential plasma samples collected from P#2 over nine
116 days during early infection showed similar binding to SARS-CoV-2 RBD and
117 NP and remained relatively stable over the course of the infection. To our surprise,
118 virtually no cross-reactivity between SARS-CoV RBD and MERS-CoV RBD

119 was detected (Figure 1A), despite strong recognition by the positive control
120 antibodies (data not shown). However, strong cross-reactivity was detected
121 against trimeric Spikes from SARS-CoV and MERS-CoV in both ELISA (Figure
122 1B) and cell-surface staining (Figure S1). All samples except P#4A
123 demonstrated significant levels of cross-binding to SARS-CoV trimeric Spike
124 while only those from P#1, P#2 and P#4B cross recognized MERS-CoV trimeric
125 Spike (Figure 1B). None of the plasma samples were reactive to HIV-1
126 envelope trimer derived from strain BG505²⁷. The same plasma samples were
127 also evaluated for neutralization of pseudoviruses bearing the Spike proteins of
128 either SARS-CoV-2, SARS-CoV, or MERS-CoV. Consistent with the antibody
129 binding results, varying degrees of neutralizing activities against SARS-CoV-2
130 were found across individuals (Figure 1C). However, cross-neutralizing against
131 SARS-CoV and MERS-CoV is rather minimal as all plasma samples tested,
132 including healthy control plasma, had negligible levels of neutralization (Figure
133 1C). No detectable neutralization was found for any plasma sample against the
134 pseudovirus control bearing the HIV-1 envelope MG04 (Figure 1C). Taken
135 together, these results suggest that RBDs from SARS-CoV-2, SARS-CoV, and
136 MERS-CoV are likely to be immunologically distinct despite substantial
137 sequence and structural similarities^{14,17}. Thus, regions beyond RBDs likely
138 contribute to the observed cross-reactivity against SARS-CoV and MERS-CoV
139 Spike protein.

140 Flow cytometry with a range of gating strategies was used to study
141 SARS-CoV-2-specific B cell responses and identity B cells recognizing
142 fluorescent-labeled RBD probes (Figure 1D and Figure S2). As shown in Figure
143 1E, the RBD-specific B cells constitute about 0.005-0.065% among the total B
144 cell population and 0.023-0.329% among the memory subpopulations. The
145 number of RBD-specific B cells are relatively higher in P#2, P#5, P#16, and
146 P#22 (Figure 1E), which appeared to correlate well with binding activity of
147 corresponding plasma samples to SARS-CoV-2 RBD and trimeric Spike protein
148 (Figure 1A and 1B). However, sample P#1A demonstrated the lowest RBD-
149 specific B cell response despite high-level plasma binding. As P#1 was the only
150 patient succumb to disease, it is uncertain whether this dichotomy of high
151 plasma binding activity and low levels of RBD-specific B cells is a surrogate

152 marker of rapid disease progression. This phenomenon needs study in a larger
153 population of samples.

154

155 **Single B cell antibody cloning and heavy chain repertoire analyses.** We
156 further isolated RBD-binding B cells into single cell suspension for cloning and
157 evaluation of the mAb response (Figure 1D and Figure S2). Immunoglobulin
158 heavy and light chains were amplified by RT-PCR using nested primers. The
159 amplified products were cloned into linear expression cassettes to produce full
160 IgG1 antibodies as previously described ^{28,29}. The number of B cell clones
161 varied from 10 to 106 among the subjects and each clone has been differentially
162 represented (Figure S3). Individual IgGs were produced by transfection of
163 linear expression cassettes and tested for SARS-CoV-2 RBD reactivity by
164 ELISA. On average, fifty-eight percent of the antibody clones were reactive,
165 although great variability was found among different individuals (Figure S3).
166 Out of 358 antibodies, we obtained 206 that bound to SARS-CoV-2 RBD with
167 165 distinct sequences (Table S2). These 206 antibodies demonstrated
168 significant differences in binding activity. For example, a large number of
169 antibodies from samples P#2B, P#2C, P#4A, P4#B, P#5A, P#16A, and P#22A
170 had OD 450 values well over 4.0, while none of those from sample P#1A
171 exceeded 4.0. There were too few antibodies from P#3A and P#8A to make
172 meaningful evaluations (Figure S3). Furthermore, samples from different study
173 subjects also demonstrated substantial differences in heavy chain variable
174 gene (VH) usage (Figure 2A). For instance, P#1 samples are dominated by
175 VH3-53, 3-13, and 1-69 which constituted approximately 21.4%, 14.3%, and
176 14.3% of the entire VH repertoire, respectively. Samples from P#2 and P#5 are
177 more diverse in distribution and frequency of their VH usage. However, no
178 single or group of VH families stood out among study subjects, suggesting
179 patients have immunologically distinct responses to SARS-CoV-2 infection.
180 This hypothesis is supported by the phylogenetic analysis of all 206 VH
181 sequences superimposed with their corresponding binding activities as
182 presented in Figure 2B. The high-binding clusters (light orange circle: 80% of
183 clusters with OD 450 > 3) were widely distributed across multiple heavy chain

184 families. In fact, majority of the high-binding antibodies were derived by clonal
185 expansion of specific VH families in P#2, P#4, and P#5. Similarly, the middle-
186 (60-80% of clusters with OD 450 > 3) and low- (< 60% cluster with OD 450 > 3)
187 binding clusters were also widely distributed and each consisted of
188 disproportionately represented VH gene families.

189 **Broad diversity and clonal expansion of antibodies in the repertoire.** As
190 P#2 showed a large number of RBD-binding antibodies and was the only
191 patient with three sequential blood samples, we conducted more detailed
192 characterization of P#2 antibodies. Among a total of 69 antibodies from P#2,
193 the majority (59%) were scattered across various branches and the remaining
194 (41%) were clonally expanded into three major clusters (Figure 3A). Antibodies
195 from the three time points (A, B, C) do not appear to group together but rather
196 interdigitate among themselves, suggesting they are highly related during early
197 infection. Three clones were significantly enriched and each constituted
198 between 12-14% of the entire tested repertoire (Figure 3A). Their heavy-chain
199 variable regions belong to the VH1-2*06, VH3-48*02, and VH3-9*01 families.
200 The corresponding light-chain kappa (Igk) belongs to 2-40*01/2D-40*01, 3-
201 20*01, and light-chain lambda (Igl) to 2-14*02 with the respective joining
202 segment kappa 4 (Jk4), Jk5 and joining segment lambda 1 (Jl1) (Table S2).
203 More importantly, these clonally expanded antibodies were identified in all three
204 samples indicating that they are strongly selected for during infection. When
205 comparing their representation within each cluster, VH1-2*06 and VH3-9*01
206 appeared to increase from approximately 33 to 45%, whereas VH3-48*02
207 decreased from 33 to 9% over the three time points, although the number of
208 clones was too small for statistical significance. Interestingly, the somatic
209 hypermutation (SHM) or germline divergence for VH1-2*06 was 0% and this
210 cluster persisted during the study period. However, the SHM for VH3-48*02
211 reached as high as 9.6% and for VH3-9*01 reached 3.8% compared to the
212 overall average of $2.2\% \pm 3.3\%$ among the 69 VH sequences. Furthermore,
213 the CDR3 length for VH1-2*06, VH3-48*02, and VH3-9*01 was 19aa, 16aa,
214 and 23aa, respectively, compared with the overall average of $16 \pm 4\text{aa}$ among
215 the 69 VH sequences. Close examination of the longest CDR3 from the

216 VH3-9*01 cluster revealed richness in tyrosine, indicating potential hydrogen
217 bonding and hydrophobic interactions with the surrounding residues. These
218 results shed light on the clonal expansion and broad diversity of RBD-specific
219 antibodies during early infection and their potential role in controlling SARS-
220 CoV-2 infection.

221

222 **Binding and neutralizing properties of selected antibodies.** We selected 13
223 of the 69 P#2 antibodies sequences based on their representation and
224 distribution on the phylogenetic tree (Figure 3A, starred). Five P#1A antibody
225 clones were used as controls. Surface plasmon resonance (SPR) with SARS-
226 CoV-2 RBD showed that P#2 antibodies had dissociation constants (Kd)
227 ranging from 10^{-8} to 10^{-9} M while those from P#1 ranged from not detectable to
228 10^{-9} M (Table 1 and Figure S4). SHM did not appear to correlate with Kd; some
229 germline clones with 0% divergence in both VH and VL genes (P2A-1A10, P2B-
230 2G4, P2C-1A3, and P2C-1E1) had Kd values comparable to clones with higher
231 levels of SHM. The Kd of representative clones (P2A-1A8, P2A-1A10, and P2A-
232 1B3) from the three clonally expanded clusters fell into a similar range,
233 suggesting that their expansion may not be driven by affinity maturation. Next,
234 we measured each antibody for competition with ACE2 for binding to the SARS-
235 CoV-2 RBD. Specifically, the RBD was covalently immobilized on a CM5 sensor
236 chip and first saturated by antibody and then flowed through with soluble ACE2.
237 Competing capacity of each antibody was measured as percent reduction in
238 ACE2 binding with the RBD (Table 1 and Figure S5). As shown in Table 1, the
239 evaluated antibodies demonstrated various competing capacity with ACE2. The
240 most powerful were P2C-1F11 and P2B-2F6, which reduced ACE2 binding
241 about 99.2% and 98.5%, respectively. Two of the three representative
242 antibodies from the clonal expanded clusters (P2A-1A10 and P2A-1B3) had
243 slightly over 80% and 90% reduction, respectively. The third representative
244 (P2A-1A8) only showed 57% reduction. Many antibodies had only limited
245 competing power with ACE2 despite impressive Kd values, suggesting binding
246 affinity is not predictive of ACE2 competing capacity. Control antibodies from
247 P#1 demonstrated even lower competing power with ACE2. Surprisingly, none
248 of the antibodies tested demonstrated cross-binding with SARS-CoV and

249 MERS-CoV RBD except P1A-1C7 ($K_d=4.85\mu M$), for which only limited cross
250 reactivity with SARS-CoV RBD was detected (Figure S4).

251 We next studied antibody neutralizing activities against pseudoviruses
252 bearing the Spike protein of SARS-CoV-2. Consistent with the competing
253 capacity findings, neutralizing activity varied considerably with IC_{50} values
254 ranging from 0.03 to $> 50 \mu g/ml$ (Figure 4B 4A and Table 1). P2C-1F11 and
255 P2B-2F6 were the most potent, followed by P2C-1A3 and P2C-1C10. Overall,
256 ACE2 competing capacity correlated well with the neutralizing activities,
257 although this correlation was not exact in some instances. Notably, no cross-
258 neutralization was found either against pseudoviruses bearing the Spike of
259 SARS-CoV or MERS-CoV (data not shown) nor with cell-surface staining of
260 trimeric SARS-CoV and MERS-CoV Spike (Figure S6). Furthermore, we
261 selected P2C-1F11, P2B-2F6, and P2C-1A3 for neutralizing activity analyses
262 against live SARS-CoV-2. Consistent with their respective pseudovirus assay
263 findings, P2C-1F11 and P2B-2F6 demonstrated potent neutralization activity
264 while that of P2C-1A3 was somewhat lower, although it needs to be noted that
265 CPE assay is not particularly quantitative (Figure 4C). Lastly, we determined
266 whether these antibodies compete for similar epitopes on the SARS-CoV-2
267 RBD. We selected a total of six antibodies with ACE2 competitive capacities of
268 at least 70% and analyzed them in a pairwise competition fashion using SPR.
269 As shown in Table 2 and Figure S7, variable degrees of competition were found
270 among the pairs of antibodies. P2C-1A3, for instance, was competitive against
271 all antibodies tested with reduction capacity ranging from 52 to 76. P2C-1F11,
272 on the other hand, was less competitive with other antibodies and in particular,
273 only minimally competitive with P2C-1C10. P2B-2F6, another potent
274 neutralizing antibody, was broadly competitive with all antibodies tested. These
275 results indicate that the antibodies analyzed recognized both overlapping and
276 distinct epitopes. Different mAbs may therefore exert their neutralizing activity
277 through different mechanisms.

278

279 **Discussion**

280 We characterized antibody responses in eight COVID-19 patients and isolated
281 206 mAbs specific to the SARS-CoV-2 RBD. Bioinformatic and biologic

characterization indicates that these antibodies are derived from broad and diverse families of antibody heavy and light chains. Each individual appears to have unique pattern of distribution in the antibody repertoire without apparent preferences for particular antibody families. Each antibody clone is also differentially represented. In P#2, for whom additional analyses were conducted, we found substantial variability in the distribution and frequency of each antibody family. Some clones were identified only once whereas others underwent high degrees of clonal expansion. Some clones were virtually identical to their germline ancestors while others became more divergent during the infection period. The CDR3 length also varied among the different clones. These differences at the genetic levels corresponded with their binding and neutralizing activities. Binding affinity (K_d) fell in the range of 10^{-8} to 10^{-9} M, equivalent to many antibodies identified during acute infections³⁰⁻³² but significantly lower than those identified during chronic HIV-1 infections³³⁻³⁵. However, binding affinity alone does not predict neutralizing activity. Competition with the receptor ACE2 governs antibody potency, although some degree of discrepancy does exist. In particular, the most potent antibodies, P2C-1F11 and P2B-2F6, out-competed ACE2 with close to 100% efficiency, indicating that blocking the RBD and ACE2 interaction is a useful surrogate for antibody neutralization. Among the antibodies tested, substantial variations in competition for similar RBD epitopes or regions were also found. The most potent antibody, P2C-1F11, did not seem target the same epitope as the relatively moderate antibody P2C-1C10. Thus, these two antibodies could be combined for synergistic antiviral effect. As we continue to screen more antibodies from P#2 and other study subjects, more potent and diverse antibodies are expected to be identified. These antibodies will serve as the best candidates for the development of prophylactic and therapeutic intervention against COVID-19 infection.

Most surprising in this study was the absence of antibody cross-reactivity with RBDs from SARS-CoV and MERS-CoV. Based on the sequential and structural similarities of RBDs from SARS-CoV-2 and SARS-CoV, we predicted some degree of cross-binding and even cross-neutralization between the two viruses. However, species-specific RBD responses in SARS-CoV-2 patients do

315 suggest that RBDs from SARS-CoV-2 and SARS-CoV are immunologically
316 distinct. If so, antibodies and vaccines must target each viral species differently
317 in order to achieve maximum efficacy in protecting the host from infection. Our
318 finding somewhat resolves the question of why many previously isolated
319 SARS-CoV antibodies failed to cross-neutralize SARS-CoV-2 despite
320 detectable levels of binding with Spike of SARS-CoV-2³⁶. The absence of cross-
321 recognition between RBDs was also apparent at the plasma level. Although
322 strong binding to SARS-CoV-2 RBD was identified, plasma samples from the
323 study subjects failed to demonstrate appreciable cross-reactivity with either
324 SARS-CoV or MERS-CoV RBD, highlighting the immunological distinctions
325 among the RBDs from the three viruses. However, substantial cross-reactivity
326 were found when the same plasma samples were applied to the trimeric Spike
327 proteins of SARS-CoV and MERS-CoV, although this was higher with the
328 former than the latter. This indicates that such cross-reactivity likely occurs in
329 regions outside the RBD. Determining whether this cross-reactive response
330 has any neutralizing or protection capacity against infection would require
331 further investigation. Finally, despite successfully isolating and characterizing a
332 large of number mAbs against SARS-CoV-2, we cannot draw any firm
333 correlation between antibody response and disease status at this time. In
334 particular, the three severe cases (P#1, P#2, and P#5) appear to have relatively
335 higher plasma binding and neutralizing activities against SARS-CoV-2 than
336 those with relative mild symptoms. A larger number of patients must be studied
337 to elucidate the drivers and impact of associations between antibody response
338 and disease progression, which will provide pivotal reference for our antibody-
339 based intervention as well as vaccine development.

340

341 **Materials and Methods**

342 **Study approval.** This study received approval from the Research Ethics
343 Committee of Shenzhen Third People's Hospital, China (approval number:
344 2020-084). The Research Ethics Committee waived the requirement informed
345 consent before the study started because of the urgent need to collect
346 epidemiological and clinical data. We analyzed all the data anonymously.

347 **Patients and blood samples.** The study enrolled a total of eight patients aged
348 10 to 66 years old infected with SARS-CoV-2 in January 2020 (Table S1). A
349 plasma sample from a healthy control was also included. Of these eight patients,
350 six (P#1 through P#4, P#8, and P#16) had Wuhan exposure history through
351 personal visit and two had direct contact with individuals from Wuhan. Four
352 subjects (P#1 through P#4) were part of a family cluster (P#1 through P#5)
353 infected while visiting Wuhan and subsequently transmitted infection to P#5
354 after returning to Shenzhen ⁵. All patients were hospitalized at Shenzhen Third
355 People's Hospital, the designated city hospital for treatment of COVID-19
356 infected patients, three to nine days after symptom onset. All patients presented
357 with fever, fatigue, and dry cough and three (P#1, P#2 and P#5) developed
358 severe pneumonia. Four patients (P#1, P#2, P#5, and P#22) were 60 years or
359 older, of which three (P#1, P#2, and P#22) had underlying disease such as
360 hypertension. SARS-CoV-2 infection status was verified by RT-PCR of
361 nasopharyngeal swab and throat swab specimens. No patient had detectable
362 influenza A, B, respiratory syncytial virus (RSV), or adenovirus co-infections.
363 Chest computed tomographic scans showed varying degrees of bilateral lung
364 patchy shadows or opacity. All patients received antiviral and corticosteroid
365 treatments, recovered and were discharged except for P#1, who succumbed to
366 disease in hospital. Single (P#1, P#3, P#5, P#8, P#16, and P#22) or sequential
367 (P#2 and P#4) blood samples were collected during hospitalization and follow-
368 up visits and separated into plasma and peripheral blood mononuclear cells
369 (PBMCs) by Ficoll-Hypaque gradient (GE Healthcare) centrifugation. All plasma
370 samples were heat-inactivated at 56 °C for 1h before being stored at -80 °C.
371 PBMCs were maintained in freezing media and stored in liquid nitrogen until
372 use.

373
374 **Recombinant RBDs and trimeric Spike from SARS-CoV-2, SARS-CoV, and**
375 **MERS-CoV and receptor ACE2.** Recombinant RBDs and trimeric Spike for
376 MERS-CoV, SARS-CoV, and SARS-CoV-2 and the N-terminal peptidase
377 domain of human ACE2 (residues Ser19-Asp615) were expressed using the
378 Bac-to-Bac baculovirus system (Invitrogen) as previously described ^{18,19,37-39}.
379 SARS-CoV-2 RBD (residues Arg319-Phe541) containing the gp67 secretion

380 signal peptide and a C-terminal 6×His tag was inserted into pFastBac-Dual
381 vectors (Invitrogen) and transformed into DH10Bac component cells. The
382 bacmid was extracted and further transfected into Sf9 cells using Cellfectin II
383 Reagents (Invitrogen). The recombinant viruses were harvested from the
384 transfected supernatant and amplified to generate high-titer virus stock. Viruses
385 were then used to infect Hi5 cells for RBD and trimeric Spike expression.
386 Secreted RBD and trimeric Spike were harvested from the supernatant and
387 purified by gel filtration chromatography as previously reported^{18,19,37-39}.

388 **ELISA analysis of plasma and antibody binding to RBD, trimeric Spike,
389 and NP proteins.** The recombinant RBDs and trimeric Spike derived from
390 SARS-CoV-2, SARS-CoV and MERS-CoV and the SARS-CoV-2 NP protein
391 (Sino Biological, Beijing) were diluted to final concentrations of 0.5 µg/ml or
392 2µg/ml, then coated onto 96-well plates and incubated at 4°C overnight.
393 Samples were washed with PBS-T (PBS containing 0.05% Tween 20) and
394 blocked with blocking buffer (PBS containing 5% skim milk and 2% BSA) at RT
395 for 1h. Either serially diluted plasma samples or isolated mAbs were added the
396 plates and incubated at 37°C for 1h. Wells were then incubated with secondary
397 anti-human IgG labeled with HRP (ZSGB-BIO, Beijing) and TMB substrate
398 (Kinghawk, Beijing) and optical density (OD) was measured by a
399 spectrophotometer at 450nm and 630nm. The serially diluted plasma from
400 healthy individuals or mAbs against SARS-CoV, MERS-CoV or HIV-1 were
401 used as controls.

402 **Isolation of RBD-specific single B cells by FACS.** RBD-specific single B
403 cells were sorted as previously described^{28,40}. In brief, PBMCs from infected
404 individuals were collected and incubated with an antibody and RBD cocktail for
405 identification of RBD-specific B cells. The cocktail consisted of CD19-PE-Cy7,
406 CD3-Pacific Blue, CD8-Pacific Blue, CD14-Pacific Blue, CD27-APC-H7, IgG-
407 FITC (BD Biosciences) and the recombinant RBD-Strep or RBD-His described
408 above. Three consecutive staining steps were conducted. The first was a
409 LIVE/DEAD Fixable Dead Cell Stain Kit (Invitrogen) in 50µl phosphate-buffered
410 saline (PBS) applied at RT for 20 minutes to exclude dead cells. The second
411 utilized an antibody and RBD cocktail for an additional 30min at 4 °C. The third

412 staining at 4 °C for 30min involved either: Streptavidin-APC (eBioscience)
413 and/or Streptavidin-PE (BD Biosciences) to target the Strep tag of RBD, or anti-
414 his-APC and anti-his-PE antibodies (Abcam) to target the His tag of RBD. The
415 stained cells were washed and resuspended in PBS before being strained
416 through a 70µm cell mesh (BD Biosciences). RBD-specific single B cells were
417 gated as CD19+CD3-CD8-CD14-IgG+RBD+ and sorted into 96-well PCR
418 plates containing 20µl of lysis buffer (5 µl of 5 x first strand buffer, 0.5 µl of
419 RNase out, 1.25 µl of 0.1 M DTT (Invitrogen) per well and 0.0625 µl of Igepal
420 (Sigma). Plates were then snap-frozen on dry ice and stored at -80 °C until RT
421 reaction.

422 **Single B cell PCR, cloning and expression of mAbs.** The IgG heavy and
423 light chain variable genes were amplified by nested PCR and cloned into linear
424 expression cassettes or expression vectors to produce full IgG1 antibodies as
425 previously described ^{29,41}. Specifically, all second round PCR primers
426 containing tag sequences were used to produce the linear Ig expression
427 cassettes by overlapping PCR. Separate primer pairs containing the specific
428 restriction enzyme cutting sites (heavy chain, 5'-Agel/3'-Sall; kappa chain, 5'-
429 Agel/3'-BsiWI; and lambda chain, 5'-Agel/3'-Xhol) were used to amplify the
430 cloned PCR products. The PCR products were purified and cloned into the
431 backbone of antibody expression vectors containing the constant regions of
432 human IgG1. Overlapping PCR products of paired heavy and light chain
433 expression cassettes were co-transfected into 293T cells (ATCC) grown in 24-
434 well plates. Antigen-specific ELISA was used to detect the binding capacity of
435 transfected culture supernatants to SARS-CoV-2 RBD. Monoclonal antibodies
436 were produced by transient transfection of 293F cells (Life Technologies) with
437 equal amounts of paired heavy and light chain plasmids. Antibodies in the
438 culture supernatant was purified by affinity chromatography using Protein A
439 beads columns (National Engineering Research Center for Biotechnology,
440 Beijing) according to the manufacturer's protocol. Concentrations were
441 determined by BCA Protein Assay Kits (Thermo Scientific). SARS-CoV, MERS-
442 CoV, and HIV-1 mAbs were also included as controls. SARS-CoV antibodies
443 (S230 and m396) previously isolated by others ⁴² were synthesized and

444 sequences verified before expression in 293T cells and purification by protein
445 A chromatography. MERS-CoV antibodies (Mab-GD33) were derived from
446 previously reported ⁴³. HIV-1 antibody VRC01 was a broadly neutralizing
447 antibody directly isolated from a patient targeting the CD4 binding site of
448 envelope glycoprotein ⁴⁰.

449 **Antibody binding kinetics, epitope mapping, and competition with**
450 **receptor ACE2 measured by SPR.** The binding kinetics and affinity of mAbs
451 to SARS-CoV-2 RBD were analyzed by SPR (Biacore T200, GE Healthcare).
452 Specifically, purified RBDs were covalently immobilized to a CM5 sensor chip
453 via amine groups in 10mM sodium acetate buffer (pH 5.0) for a final RU around
454 250. SPR assays were run at a flow rate of 30ml/min in HEPE buffer. The
455 sensograms were fit in a 1:1 binding model with BIA Evaluation software (GE
456 Healthcare). For epitope mapping, two different antibodies were sequentially
457 injected and monitored for binding activity to determine whether the two mAbs
458 recognized separate or closely-situated epitopes. To determine competition
459 with the human ACE2 peptidase domain, SARS-CoV-2 RBD was immobilized
460 to a CM5 sensor chip via amine group for a final RU around 250. Antibodies (1
461 μ M) were injected onto the chip until binding steady-state was reached. ACE2
462 (2 μ M), which was produced and purified as above, was then injected for 60
463 seconds. Blocking efficacy was determined by comparison of response units
464 with and without prior antibody incubation.

465 **Analysis of plasma and antibody binding to cell surface expressed**
466 **trimeric Spike protein.** HEK 293T cells were transfected with expression
467 plasmid encoding the full length spike of SARS-CoV-2, SARS-CoV or MERS-
468 CoV and incubated at 37 °C for 36 h. The cells were digested with trypsin and
469 distributed into 96 well plates for the individual staining. Cells were washed
470 twice with 200 μ l staining buffer (PBS with 2% heated-inactivated FBS) between
471 each following steps. The cells were stained at room temperature for 30
472 minutes in 100 μ l staining buffer with 1:100 dilutions of plasma or 20 μ g/ml
473 monoclonal antibodies. The cells were then stained with PE labeled anti-human
474 IgG Fc secondary antibody (Biolegend) at a 1:20 dilution in 50 μ l staining buffer
475 at room temperature for 30 minutes. Finally, the cells were re-suspended and

476 analyzed with FACS Calibur instrument (BD Biosciences, USA) and FlowJo 10
477 software (FlowJo, USA). HEK 293T cells without transfection were also stained
478 as background control. S230 and m396 targeting the RBD of SARS-CoV spike
479 ⁴² and Mab-GD33 targeting the RBD of MERS-CoV spike ⁴³ were used as
480 positive primary antibody controls, while VRC01 targeting HIV-1 env ⁴⁰ was
481 used as an irrelevant primary antibody control.

482 **Neutralization activity of mAbs against pseudovirus and live SARS-CoV-2.**
483 SARS-CoV-2, SARS-CoV and MERS-CoV pseudovirus were generated by co-
484 transfection of human immunodeficiency virus backbones expressing firefly
485 luciferase (pNL43R-E-luciferase) and pcDNA3.1 (Invitrogen) expression
486 vectors encoding the respective S proteins into 293T cells (ATCC) ^{37,38,44,45}.
487 Viral supernatants were collected 48 h later. Viral titers were measured as
488 luciferase activity in relative light units (Bright-Glo Luciferase Assay Vector
489 System, Promega Biosciences). Control envelope glycoproteins derived from
490 human immunodeficiency virus (HIV)-1 and their corresponding pseudoviruses
491 were produced in the same manner. Control mAbs included VRC01 against
492 HIV-1 ⁴⁰; S230 and m396 against SARS-CoV ⁴²; and Merb-GD33 against
493 MERS-CoV ⁴³. Neutralization assays were performed by incubating
494 pseudoviruses with serial dilutions of purified mAbs at 37°C for 1h. Huh7 cells
495 (ATCC) (approximately 1.5×10^4 per well) were added in duplicate to the virus-
496 antibody mixture. Half-maximal inhibitory concentrations (IC₅₀) of the evaluated
497 mAbs were determined by luciferase activity 48h after exposure to virus-
498 antibody mixture using GraphPad Prism 6 (GraphPad Software Inc.).

499 All experiments involving live SARS-CoV-2 followed approved Biosafety
500 Level 3 laboratory standard operating procedures. Neutralization assays
501 against live SARS-CoV-2 were conducted using a clinical isolate
502 (Beta/Shenzhen/SZTH-003/2020, EPI_ISL_406594 at GISAID) previously
503 obtained from a nasopharyngeal swab of P#3. The isolate was amplified in Vero
504 cell lines to make working stocks of the virus (1×10^5 PFU/ml). To analyze the
505 mAb neutralizing activities, Vero E6 cells were seeded at 10^4 /well in 96-well
506 culture plates and cultured at 37 °C to form a monolayer. Serial dilutions of
507 mAbs were mixed separately with 100 PFU of SARS-CoV-2, incubated at 37 °C

508 for 1 h, and added to the monolayer of Vero E6 cells in duplicates. Cells either
509 unexposed to the virus or mixed with 100 PFU SARS-CoV-2 were used as
510 negative (uninfected) and positive (infected) controls, respectively. Cytopathic
511 effects (CPE) were observed daily and recorded on Day 2 post-exposure.

512 **Gene family usage and phylogenetic analysis of mAbs.** The program
513 IMGT/V-QUEST (http://www.imgt.org/IMGT_vquest/vquest) was used to
514 analyze germline gene, germline divergence or degree of somatic
515 hypermutation (SHM), the framework region (FR) and the loop length of the
516 complementarity determining region 3 (CDR3) for each antibody clone. The IgG
517 heavy and light chain variable genes were aligned using Clustal W in the
518 BioEdit sequence analysis package (<https://bioedit.software.informer.com/7.2/>).
519 Phylogenetic analyses were performed by the Maximum Likelihood method
520 using MEGA X (Molecular Evolutionary Genetics Analysis across computing
521 platforms). Several forms of the phylogenetic trees are presented for clarity.

522 **Antibody production.** The production of antibodies was conducted as
523 previously described ^{38,46}. The genes encoding the heavy and light chains of
524 isolated antibodies were separately cloned into expression vectors containing
525 IgG1 constant regions and the vectors were transiently transfected into
526 HEK293T or 293F cells using polyethylenimine (PEI) (Sigma). After 72h, the
527 antibodies secreted into the supernatant were collected and captured by
528 protein A Sepharose (GE Healthcare). The bound antibodies were eluted and
529 further purified by gel-filtration chromatography using a Superdex 200 High
530 Performance column (GE Healthcare). The purified antibodies were either used
531 in binding and neutralizing assays.

532 **Acknowledgments** We acknowledge the work and contribution of all the health
533 providers from Shenzhen Third People's Hospital. We also thank patients for
534 their active participation. This study was supported by Bill & Melinda Gates
535 Foundation, the Science and Technology Innovation Committee of Shenzhen
536 Municipality (20200207300002), and by Tsinghua University Initiative
537 Scientific Research Program (20201080053). This work is also partially
538 supported by the National Natural Science Foundation Award (81530065),

539 Beijing Municipal Science and Technology Commission (171100000517-001
540 and -003), Beijing Advanced Innovation Center for Structural Biology at
541 Tsinghua University, the National Key Plan for Scientific Research and
542 Development of China (grant number 2016YFD0500307), Tencent Foundation,
543 Shuidi Foundation, and TH Capital. The funders had no role in study design,
544 data collection, data analysis, data interpretation, or writing of the report.

545 **Author contributions** LZ, ZZ, LL and SZ conceived and designed the study.
546 BJ and QZ performed most of the experiments together with assistance from
547 XG, RW, JY, SS, BJ, SS, and XS. XT performed live SARS-CoV-2
548 neutralization assay. JY, JG, JL, XW provided assistance in RBD and trimeric
549 Spike protein production. JY and LL played critical roles in recruitment and
550 clinical management of the study subjects. HW and JZ are in charge of sample
551 collection and processing. YW provides additional pseudovirus assay for
552 measuring neutralizing activity against SARS-CoV-2. BJ, QZ, ZZ and LZ had
553 full access to data in the study, generated figures and tables, and take
554 responsibility for the integrity and accuracy of the data presentation. LZ and ZZ
555 wrote the manuscript. All authors reviewed and approved the final version of
556 the manuscript.

557 **Data availability statements** We are happy to share reagents and information
558 presented in this study upon request.

559 **Conflict of interests:** We declare no competing interest.

560

561

562 **Figure Legends**

563

564 **Figure 1. Analyses of plasma and B cell responses specific to SARS-CoV-**

565 **2.** Serial dilutions of plasma samples were analyzed for binding to the (A) RBDs
566 or (B) trimeric Spikes of SARS-CoV-2, SARS-CoV and MERS-CoV by ELISA
567 and (C) for neutralizing activity against pseudoviruses bearing envelope
568 glycoprotein of SARS-CoV-2, SARS-CoV and MERS-CoV. Binding to SARS-
569 CoV-2 NP protein was also evaluated (A). All results were derived from at least
570 two independent experiments. (D) Gating strategy for analysis and isolation of
571 RBD-specific memory B cells and (E) their representation among the total and
572 memory subpopulation of B cells in the eight study subjects. Samples were
573 named as either A, B, or C depending on collection sequence. FSC-W, forward
574 scatter width; FSC-A, forward scatter area; and SSC-A side scatter area.

575

576 **Figure 2. Heavy chain repertoires of SARS-CoV-2 RBD-specific antibodies**

577 **analyzed (A) by individual subject or (B) across the eight subjects.** (A)
578 Distribution and frequency of heavy chain variable (VH) genes usage in each
579 subject shown along the horizontal bar. The same color scheme is used for
580 each VH family across all study subjects. The VHs that dominate across
581 isolated antibodies are indicated by actual frequencies in their respective color
582 boxes. The number of RBD-binding antibodies versus total antibodies isolated
583 are shown on the right. (B) Clustering of VH genes and their association with
584 ELISA binding activity across the eight subjects. Unrooted phylogenetic tree
585 depicting the genetic relationships among all VH genes of the RBD-binding
586 antibodies. Branch lengths are drawn to scale so that sequence relatedness
587 can be readily assessed. Sequences from the same study subject are shown
588 in the same color at the branch tips. Colored circles represent the proportion
589 (light orange, > 80%; light yellow, 60%-80%; light green < 60%) of VH clusters
590 that bind to SARS-CoV-2 RBD with OD 450 values larger than 3. The VH gene
591 families for the highest binding clusters are shown.

592

593 **Figure 3. Clonal expansion of specific heavy and light chain families in**
594 **the P#2 antibody repertoire.** (A) Phylogenetic analysis of VH (left) and VL

595 (right) genes for all RBD-binding antibodies. Clonal expanded VH and VL
596 clusters are paired and highlighted in three different colors. Branch lengths are
597 drawn to scale so that sequence relatedness can be readily assessed. (B)
598 Clonal expansion in relation to members of other VH and VL families based on
599 somatic hypermutations (SHM) and CDR3 loop lengths. For the pie charts of
600 VH (left) and VL (right) genes, the radii represent the CDR3 loop length and the
601 color scale indicates the degree of SHM. Heavy and light chain repertoires for
602 each antibody are shown along the pie circles.

603

604 **Figure 4. Antibody neutralization analyzed by pseudovirus and live SARS-
605 CoV-2.** (A) Quality control of antibody through ELISA analysis prior to
606 neutralization assay. A serial dilution of each antibody was evaluated against
607 SARS-CoV-2 RBD coated on the ELISA plate and their binding activity was
608 recorded at an optical density (OD) of 450nm and 630nm. (B-C) Antibody
609 neutralization analyzed by pseudovirus (B) or live SARS-CoV-2 (C). A serial
610 dilution of each antibody was tested against pseudovirus while two dilutions
611 against live SARS-CoV-2. Cytopathic effects (CPE) were observed daily and
612 recorded on Day 2 post-exposure. Selected antibodies and their concentrations
613 tested are indicated at the upper left corner.

614

615 **Figure S1. Analysis of plasma binding to cell surface expressed trimeric
616 Spike protein.** HEK 293T cells transfected with expression plasmid encoding
617 the full length spike of SARS-CoV-2, SARS-CoV or MERS-CoV were incubated
618 with 1:100 dilutions of plasma from the study subjects. The cells were then
619 stained with PE labeled anti-human IgG Fc secondary antibody and analyzed
620 by FACS. Positive control antibodies include S230 and m396 targeting the RBD
621 of SARS-CoV Spike, and Mab-GD33 targeting the RBD of MERS-CoV Spike.
622 VRC01 is negative control antibody targeting HIV-1 envelope glycoprotein.

623

624 **Figure S2. RBD-specific memory B cells analyzed and isolated through
625 FACS.** The recombinant RBD was labeled with either a Strep or His tag and
626 used alone or in combination to identify and isolate RBD-specific single B cells
627 through staining with the Streptavidin-APC and/or Streptavidin-PE, or anti-His-

628 APC and anti-His-PE antibodies. B cells to be isolated are highlighted in boxes
629 or ovals. Samples were named as either A, B, or C depending on collection
630 sequence. FSC-W, forward scatter width; FSC-A, forward scatter area; and
631 SSC-A side scatter area.

632

633 **Figure S3. ELISA screening of SARS-CoV-2 RBD-specific antibodies in**
634 **the supernatant of transfected cells.** The study subjects and the date of
635 sampling are indicated on the top. Samples were named as either A, B, or C
636 depending on collection sequence. Antibodies tested for each sample are
637 aligned in one vertical column whenever possible. For each evaluated antibody,
638 at least two independent measurements were performed and are presented
639 adjacently on the same row. Binding activities were assessed by OD 450 and
640 indicated by the color scheme on the right. Negatives (no binding activity) are
641 shown in gray for OD 450 values less than 0.1.

642

643 **Figure S4. Binding kinetics of isolated mAbs with SARS-CoV-2 RBD**
644 **measured by SPR.** The purified soluble SARS-CoV-2 RBD were covalently
645 immobilized onto a CM5 sensor chip followed by injection of individual antibody
646 at four or five different concentrations. The black lines indicate the
647 experimentally derived curves while the red lines represent fitted curves based
648 on the experimental data.

649

650 **Figure S5. Antibody and ACE2 competition for binding to SARS-CoV-2**
651 **RBD measured by SPR.** The sensorgrams show distinct binding patterns of
652 ACE2 to SARS-CoV-2 RBD with (red curve) or without (black curve) prior
653 incubation with each testing antibody. The competition capacity of each
654 antibody is indicated by the level of reduction in response unit of ACE2
655 comparing with or without prior antibody incubation.

656

657 **Figure S6. Analysis of antibody binding to cell surface expressed trimeric**
658 **Spike protein.** HEK 293T cells transfected with expression plasmid encoding
659 the full length spike of SARS-CoV-2, SARS-CoV or MERS-CoV were incubated

660 with 20ug/ml testing antibodies. The cells were then stained with PE labeled
661 anti-human IgG Fc secondary antibody and analyzed by FACS. Positive control
662 antibodies include S230 and m396 targeting the RBD of SARS-CoV Spike, and
663 Mab-GD33 targeting the RBD of MERS-CoV Spike. VRC01 is the negative
664 control antibody targeting HIV-1 envelope glycoprotein.

665

666 **Figure S7. Epitope mapping through competitive binding measured by**
667 **SPR.** The sensorgrams show distinct binding patterns when pairs of testing
668 antibodies were sequentially applied to the purified SARS-CoV-2 RBD
669 covalently immobilized onto a CM5 sensor chip. The level of reduction in
670 response unit comparing with or without prior antibody incubation is the key
671 criteria for determining the two mAbs recognize the separate or closely situated
672 epitopes.

673

674

675

676 **References**

677 1 Li, Q. *et al.* Early Transmission Dynamics in Wuhan, China, of Novel Coronavirus-
678 Infected Pneumonia. *N Engl J Med*, 10.1056/NEJMoa2001316,
679 doi:10.1056/NEJMoa2001316 (2020).

680 2 Zhou, P. *et al.* A pneumonia outbreak associated with a new coronavirus of probable
681 bat origin. *Nature* **579**, 270-273, doi:10.1038/s41586-020-2012-7 (2020).

682 3 Zhu, N. *et al.* A Novel Coronavirus from Patients with Pneumonia in China, 2019. *N
683 Engl J Med* **382**, 727-733, doi:10.1056/NEJMoa2001017 (2020).

684 4 Wu, F. *et al.* A new coronavirus associated with human respiratory disease in China.
685 *Nature* **579**, 265-269, doi:10.1038/s41586-020-2008-3 (2020).

686 5 Chan, J. F.-W. *et al.* A familial cluster of pneumonia associated with the 2019 novel
687 coronavirus indicating person-to-person transmission: a study of a family cluster.
688 *Lancet* **395**, 514-523, doi:10.1016/S0140-6736(20)30154-9 (2020).

689 6 Guan, W.-J. *et al.* Clinical Characteristics of Coronavirus Disease 2019 in China. *N Engl
690 J Med*, 10.1056/NEJMoa2002032, doi:10.1056/NEJMoa2002032 (2020).

691 7 Huang, C. *et al.* Clinical features of patients infected with 2019 novel coronavirus in
692 Wuhan, China. *Lancet* **395**, 497-506, doi:10.1016/S0140-6736(20)30183-5 (2020).

693 8 Wang, D. *et al.* Clinical Characteristics of 138 Hospitalized Patients With 2019 Novel
694 Coronavirus-Infected Pneumonia in Wuhan, China. *JAMA*, e201585,
695 doi:10.1001/jama.2020.1585 (2020).

696 9 Chinazzi, M. *et al.* The effect of travel restrictions on the spread of the 2019 novel
697 coronavirus (COVID-19) outbreak. *Science*, eaba9757, doi:10.1126/science.aba9757
698 (2020).

699 10 Lu, R. *et al.* Genomic characterisation and epidemiology of 2019 novel coronavirus:
700 implications for virus origins and receptor binding. *Lancet* **395**, 565-574,
701 doi:10.1016/S0140-6736(20)30251-8 (2020).

702 11 Wu, A. *et al.* Genome Composition and Divergence of the Novel Coronavirus (2019-
703 nCoV) Originating in China. *Cell Host Microbe*, S1931-3128(1920)30072-X,
704 doi:10.1016/j.chom.2020.02.001 (2020).

705 12 Ge, X.-Y. *et al.* Isolation and characterization of a bat SARS-like coronavirus that uses
706 the ACE2 receptor. *Nature* **503**, 535-538, doi:10.1038/nature12711 (2013).

707 13 Hoffmann, M. *et al.* SARS-CoV-2 Cell Entry Depends on ACE2 and TMPRSS2 and Is
708 Blocked by a Clinically Proven Protease Inhibitor. *Cell*, S0092-8674(0020)30229-30224,
709 doi:10.1016/j.cell.2020.02.052 (2020).

710 14 Walls, A. C. *et al.* Structure, Function, and Antigenicity of the SARS-CoV-2 Spike
711 Glycoprotein. *Cell*, S0092-8674(0020)30262-30262, doi:10.1016/j.cell.2020.02.058
712 (2020).

713 15 Du, L. *et al.* The spike protein of SARS-CoV--a target for vaccine and therapeutic
714 development. *Nat Rev Microbiol* **7**, 226-236, doi:10.1038/nrmicro2090 (2009).

715 16 Li, F. Structure, Function, and Evolution of Coronavirus Spike Proteins. *Annu Rev Virol*
716 **3**, 237-261, doi:10.1146/annurev-virology-110615-042301 (2016).

717 17 Wrapp, D. *et al.* Cryo-EM structure of the 2019-nCoV spike in the prefusion
718 conformation. *Science*, eabb2507, doi:10.1126/science.abb2507 (2020).

719 18 Gui, M. *et al.* Cryo-electron microscopy structures of the SARS-CoV spike glycoprotein
720 reveal a prerequisite conformational state for receptor binding. *Cell Res* **27**, 119-129,
721 doi:10.1038/cr.2016.152 (2017).

722 19 Song, W., Gui, M., Wang, X. & Xiang, Y. Cryo-EM structure of the SARS coronavirus
723 spike glycoprotein in complex with its host cell receptor ACE2. *PLoS Pathog* **14**,
724 e1007236-e1007236, doi:10.1371/journal.ppat.1007236 (2018).

725 20 Kirchdoerfer, R. N. *et al.* Stabilized coronavirus spikes are resistant to conformational
726 changes induced by receptor recognition or proteolysis. *Sci Rep* **8**, 15701-15701,
727 doi:10.1038/s41598-018-34171-7 (2018).

728 21 Yuan, Y. *et al.* Cryo-EM structures of MERS-CoV and SARS-CoV spike glycoproteins
729 reveal the dynamic receptor binding domains. *Nat Commun* **8**, 15092-15092,
730 doi:10.1038/ncomms15092 (2017).

731 22 Wan, Y., Shang, J., Graham, R., Baric, R. S. & Li, F. Receptor recognition by novel
732 coronavirus from Wuhan: An analysis based on decade-long structural studies of SARS.
733 *J Virol*, JVI.00127-00120, doi:10.1128/JVI.00127-20 (2020).

734 23 Kruse, R. L. Therapeutic strategies in an outbreak scenario to treat the novel
735 coronavirus originating in Wuhan, China. *F1000Res* **9**, 72-72,
736 doi:10.12688/f1000research.22211.2 (2020).

737 24 Li, W. *et al.* Angiotensin-converting enzyme 2 is a functional receptor for the SARS
738 coronavirus. *Nature* **426**, 450-454, doi:10.1038/nature02145 (2003).

739 25 Hamming, I. *et al.* The emerging role of ACE2 in physiology and disease. *J Pathol* **212**,
740 1-11, doi:10.1002/path.2162 (2007).

741 26 Xu, J. *et al.* Antibodies and vaccines against Middle East respiratory syndrome
742 coronavirus. *Emerg Microbes Infect* **8**, 841-856, doi:10.1080/22221751.2019.1624482
743 (2019).

744 27 Sanders, R. W. *et al.* Stabilization of the soluble, cleaved, trimeric form of the envelope
745 glycoprotein complex of human immunodeficiency virus type 1. *J Virol* **76**, 8875-8889,
746 doi:10.1128/jvi.76.17.8875-8889.2002 (2002).

747 28 Kong, L. *et al.* Key gp120 Glycans Pose Roadblocks to the Rapid Development of
748 VRC01-Class Antibodies in an HIV-1-Infected Chinese Donor. *Immunity* **44**, 939-950,
749 doi:10.1016/j.jimmuni.2016.03.006 (2016).

750 29 Liao, H.-X. *et al.* High-throughput isolation of immunoglobulin genes from single
751 human B cells and expression as monoclonal antibodies. *J Virol Methods* **158**, 171-179,
752 doi:10.1016/j.jviromet.2009.02.014 (2009).

753 30 Yu, L. *et al.* Delineating antibody recognition against Zika virus during natural infection.
754 *JCI Insight* **2**, e93042, doi:10.1172/jci.insight.93042 (2017).

755 31 Corti, D. & Lanzavecchia, A. Broadly neutralizing antiviral antibodies. *Annu Rev
756 Immunol* **31**, 705-742, doi:10.1146/annurev-immunol-032712-095916 (2013).

757 32 Stettler, K. *et al.* Specificity, cross-reactivity, and function of antibodies elicited by Zika
758 virus infection. *Science* **353**, 823-826, doi:10.1126/science.aaf8505 (2016).

759 33 Scheid, J. F. *et al.* Broad diversity of neutralizing antibodies isolated from memory B
760 cells in HIV-infected individuals. *Nature* **458**, 636-640, doi:10.1038/nature07930
761 (2009).

762 34 Wu, X. *et al.* Focused evolution of HIV-1 neutralizing antibodies revealed by structures
763 and deep sequencing. *Science* **333**, 1593-1602, doi:10.1126/science.1207532 (2011).

764 35 Liao, H.-X. *et al.* Co-evolution of a broadly neutralizing HIV-1 antibody and founder
765 virus. *Nature* **496**, 469-476, doi:10.1038/nature12053 (2013).

766 36 Tian, X. *et al.* Potent binding of 2019 novel coronavirus spike protein by a SARS
767 coronavirus-specific human monoclonal antibody. *Emerg Microbes Infect* **9**, 382-385,
768 doi:10.1080/22221751.2020.1729069 (2020).

769 37 Wang, N. *et al.* Structure of MERS-CoV spike receptor-binding domain complexed with
770 human receptor DPP4. *Cell Res* **23**, 986-993, doi:10.1038/cr.2013.92 (2013).

771 38 Jiang, L. *et al.* Potent neutralization of MERS-CoV by human neutralizing monoclonal
772 antibodies to the viral spike glycoprotein. *Sci Transl Med* **6**, 234ra259-234ra259,
773 doi:10.1126/scitranslmed.3008140 (2014).

774 39 Zhang, S. *et al.* Structural Definition of a Unique Neutralization Epitope on the
775 Receptor-Binding Domain of MERS-CoV Spike Glycoprotein. *Cell Rep* **24**, 441-452,
776 doi:10.1016/j.celrep.2018.06.041 (2018).

777 40 Wu, X. *et al.* Rational design of envelope identifies broadly neutralizing human
778 monoclonal antibodies to HIV-1. *Science* **329**, 856-861, doi:10.1126/science.1187659
779 (2010).

780 41 Tiller, T. *et al.* Efficient generation of monoclonal antibodies from single human B cells
781 by single cell RT-PCR and expression vector cloning. *J Immunol Methods* **329**, 112-124,
782 doi:10.1016/j.jim.2007.09.017 (2008).

783 42 Zhu, Z. *et al.* Potent cross-reactive neutralization of SARS coronavirus isolates by
784 human monoclonal antibodies. *Proc Natl Acad Sci U S A* **104**, 12123-12128,
785 doi:10.1073/pnas.0701000104 (2007).

786 43 Niu, P. *et al.* Ultrapotent Human Neutralizing Antibody Repertoires Against Middle
787 East Respiratory Syndrome Coronavirus From a Recovered Patient. *J Infect Dis* **218**,
788 1249-1260, doi:10.1093/infdis/jiy311 (2018).

789 44 Jia, W. *et al.* Single intranasal immunization with chimpanzee adenovirus-based
790 vaccine induces sustained and protective immunity against MERS-CoV infection.
791 *Emerg Microbes Infect* **8**, 760-772, doi:10.1080/22221751.2019.1620083 (2019).

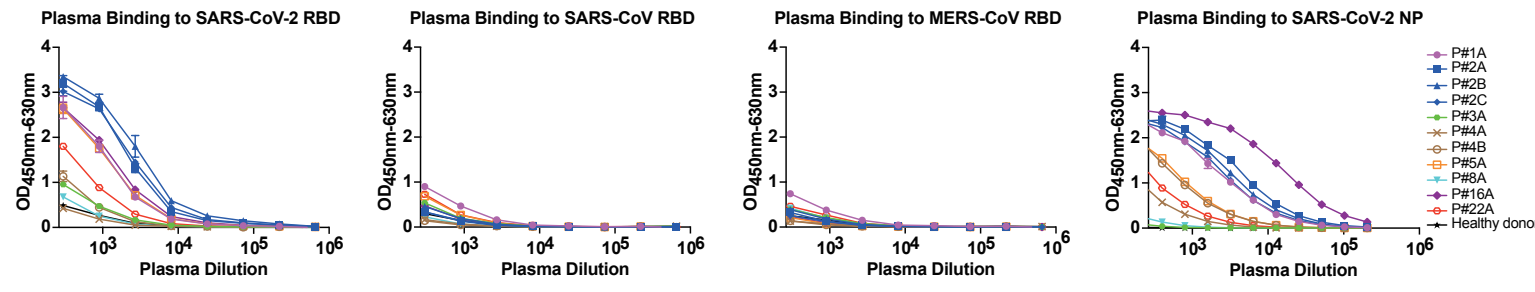
792 45 Zhang, L. *et al.* Antibody responses against SARS coronavirus are correlated with
793 disease outcome of infected individuals. *J Med Virol* **78**, 1-8, doi:10.1002/jmv.20499
794 (2006).

795 46 Zhang, Q. *et al.* Potent neutralizing monoclonal antibodies against Ebola virus
796 infection. *Sci Rep* **6**, 25856-25856, doi:10.1038/srep25856 (2016).

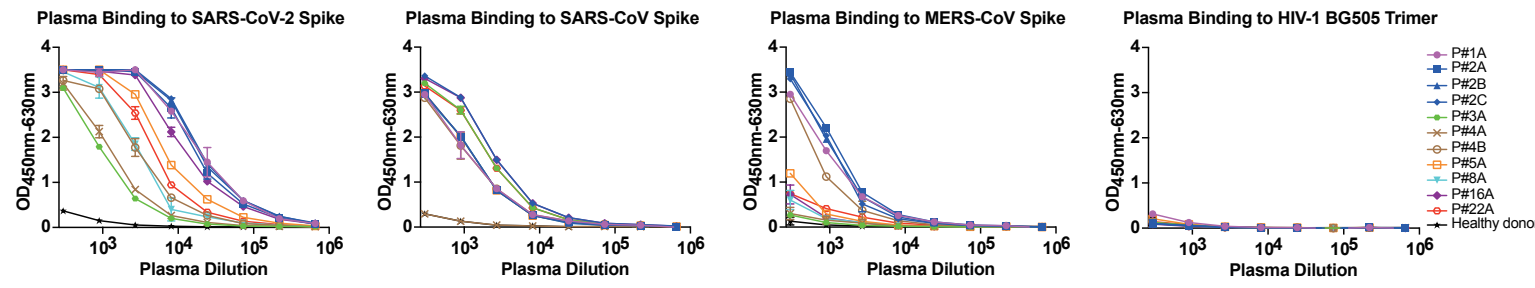
797

Figure 1

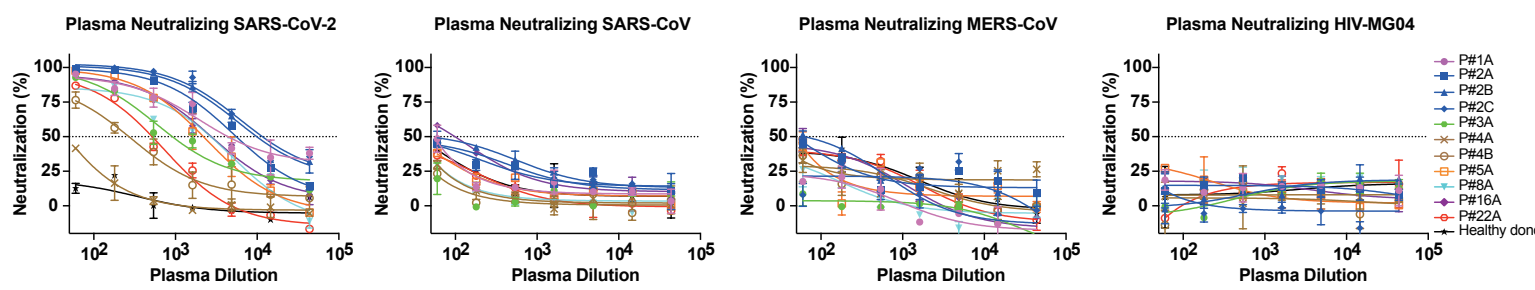
A



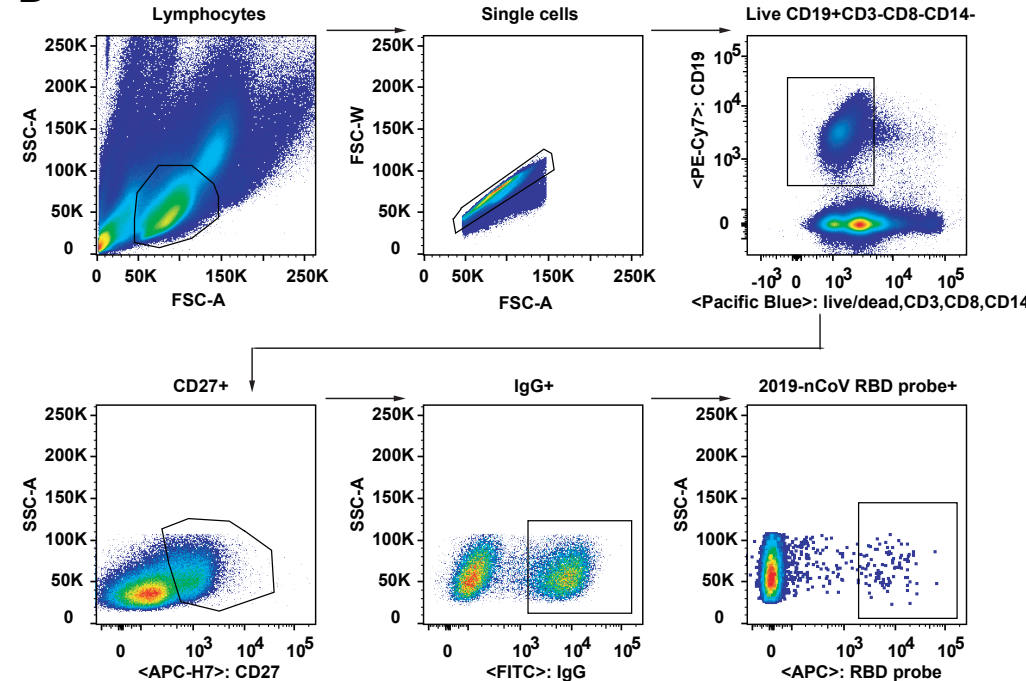
B



C



D



E

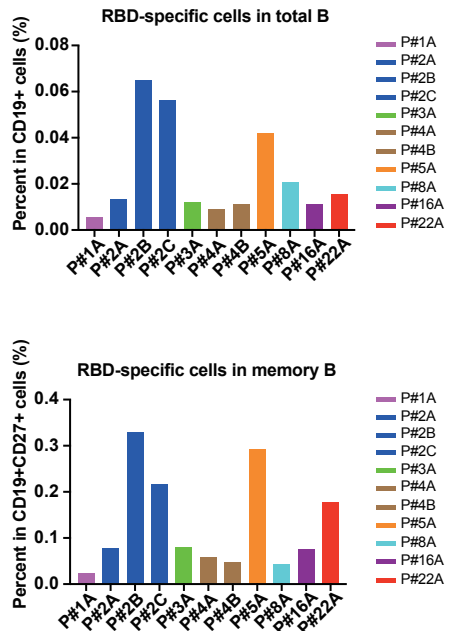


Figure 2

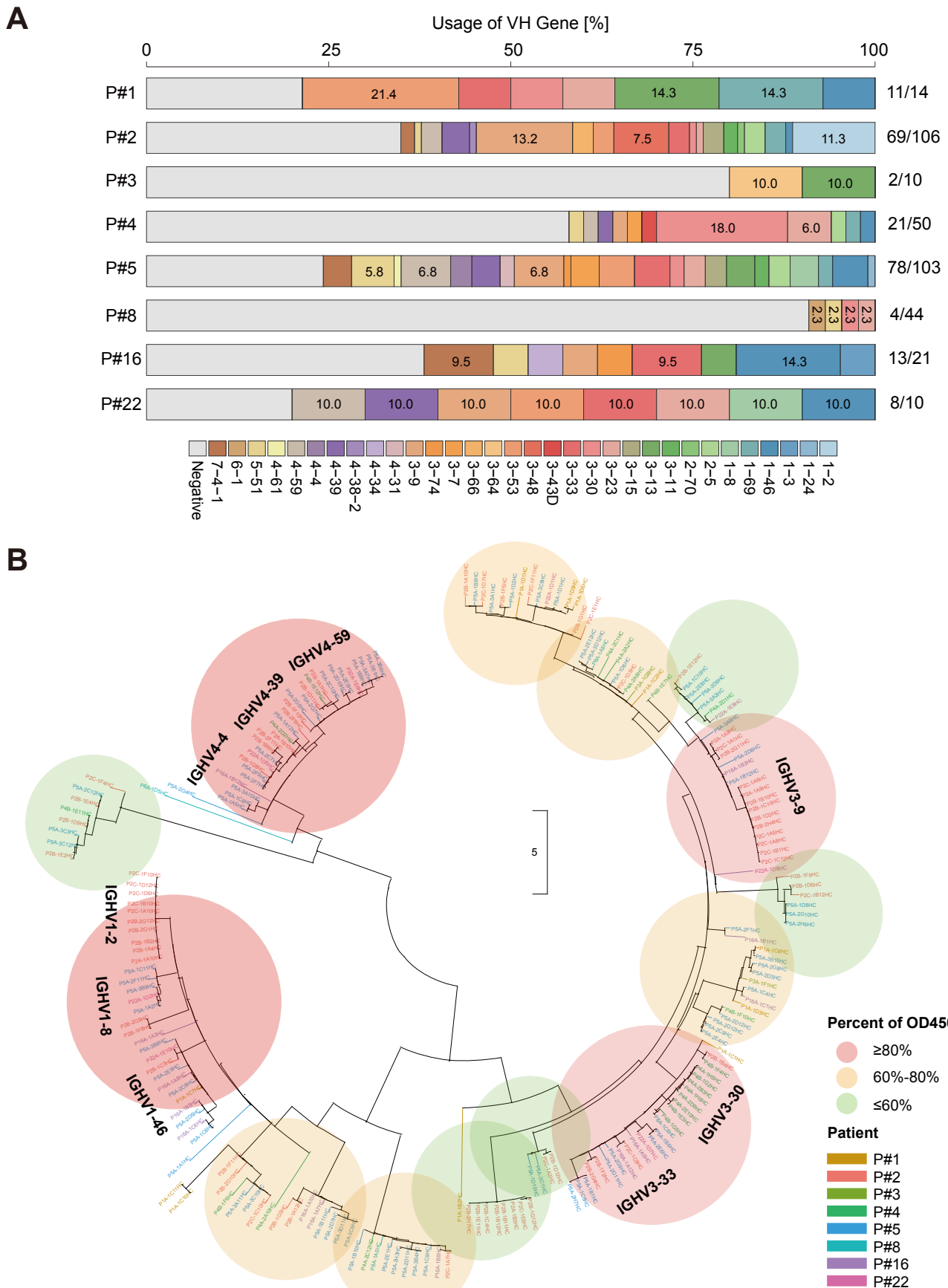


Figure 3

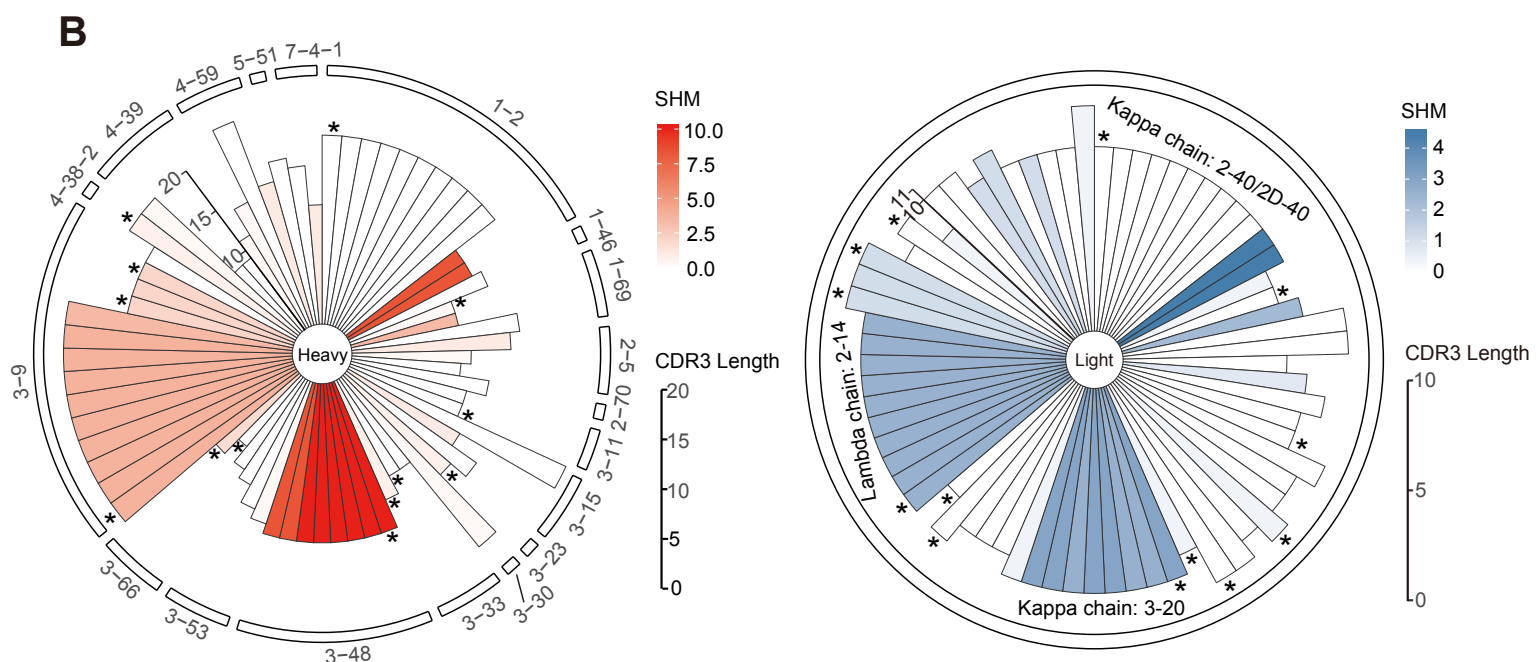
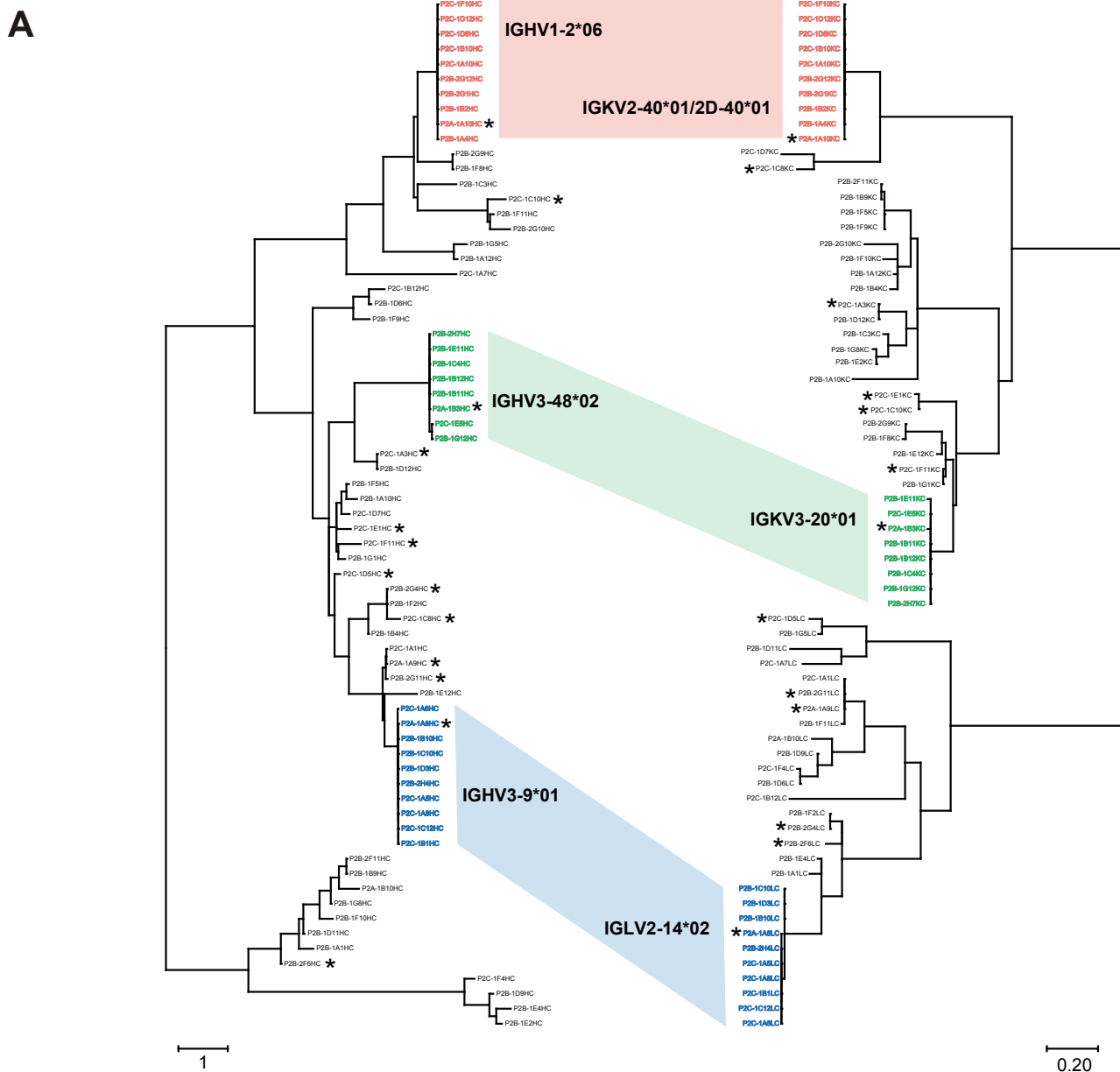


Figure 4

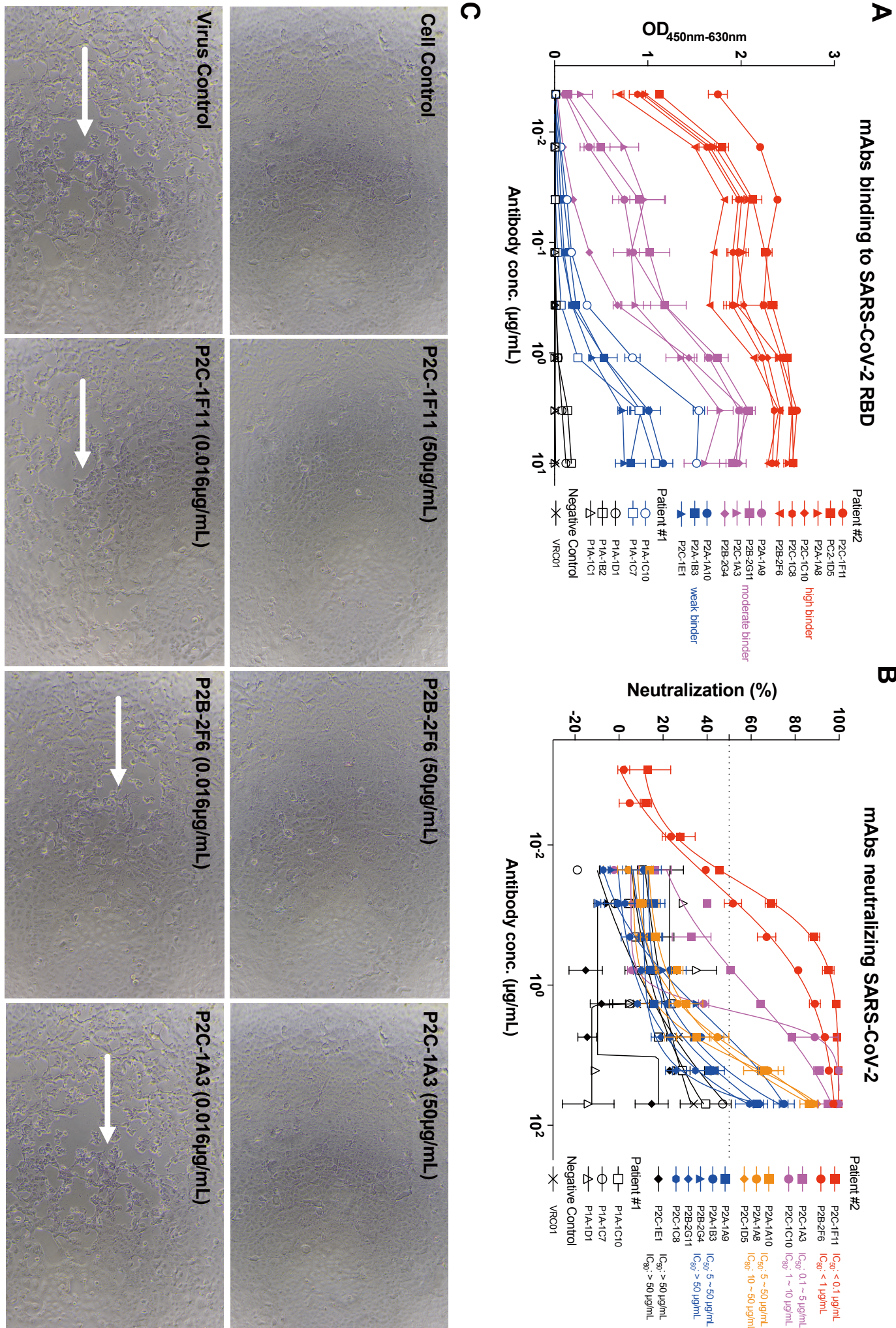


Table 1. Binding capacity, neutralizing activity, and heavy chain gene family analysis of 18 monoclonal Abs isolated from Patient #1 and Patient #2.

Patient	mAbs	Binding to RBD		Pseudovirus neutralization		Gene family analysis					
		Kd (nM)	competing w/ ACE2	IC ₅₀ (μg/ml)	IC ₈₀ (μg/ml)	IGHV	IGHJ	IGHD	CDR3 length	SHM (%)	
P#1	P1A-1C7	51.08	-5.88	>50	>50	1-46*01,1-46*03	4*02	2-2*01	15	0.00	
	P1A-1C10	8.48	24.51	>50	>50	1-69*09	4*02	3-3*01	16	10.42	
	P1A-1B2	n.d.	n.d.	n.d.	n.d.	3-30*03,3-30*18,3-30*5*01	4*02	5-24*01	12	11.46	
	P1A-1C1	n.d.	n.d.	n.d.	n.d.	3-33*01,3-33*05,3-33*06	4*02	3-10*01	17	6.25	
P1A-1D1	260.50	6.20	>50	>50	3-53*01	4*02	6-13*01	12	4.21		
P2A-1A10	4.65	80.65	8.57	39.44	1-2*06	2*01	2-2*01	19	0.00		
P2C-1C10	15.23	71.17	2.62	4.64	1-69*01,1-69D*01	4*02	4-23*01	11	0.35		
P2C-1A3	2.47	81.21	0.62	5.94	3-11*04	5*01,5*02	6-13*01	12	0.00		
P2C-1D5	1.64	17.61	10.65	25.36	3-23*04	4*02	3-10*01	14	0.69		
P2B-2G4	21.29	41.03	5.11	>50	3-33*01,3-33*06	4*02	5-18*01	11	0.00		
P2C-1C8	8.76	74.45	34.38	>50	3-33*01,3-33*06	4*02	3-22*01	13	0.69		
P#2	P2A-1B3	6.00	92.15	16.77	>50	3-48*02	5*02	3-10*01	16	10.07	
	P2C-1E1	14.99	56.61	>50	>50	3-66*01,3-66*04	4*02	5-12*01	9	0.00	
	P2C-1F11	2.12	99.17	0.03	0.12	3-66*01,3-66*04	6*02	2-15*01	11	1.75	
	P2A-1A8	8.91	57.06	7.68	26.41	3-9*01	6*02	5-12*01	23	3.82	
P2A-1A9	15.18	53.60	26.27	>50	3-9*01	6*02	3-22*01	17	2.08		
P2B-2G11	17.57	52.28	34.84	>50	3-9*01	6*02	1-26*01	17	2.08		
P2B-2F6	5.14	98.50	0.05	0.61	4-38*2*02	3*02	2-2*01	20	0.69		

The program IMGT/TV-QUEST was applied to analyze gene germline, complementarity determining region (CDR) 3 length, and somatic hypermutation (SHM). The CDR3 length was calculated from amino acids sequences. The SHM frequency was calculated from the mutated nucleotides. n.d.: not detectable.

Table 2. Epitope mapping of mAbs through competitive binding to SARS-CoV-2 RBD

mAbs	P2C-1A3	P2C-1C10	P2C-1F11	P2B-2F6	P2A-1B3	P2A-1A10
P2C-1A3		68.41	57.44	76.73	65.20	n.a.
P2C-1C10	75.33		-0.32	49.69	42.98	n.a.
P2C-1F11	52.05	-2.31		42.65	5.98	n.a.
P2B-2F6	74.87	70.97	30.22		52.79	n.a.
P2A-1B3	57.94	63.83	14.35	51.88		n.a.
P2A-1A10	76.31	84.27	79.50	73.92	42.19	

n.a.: not applicable

Figure S1

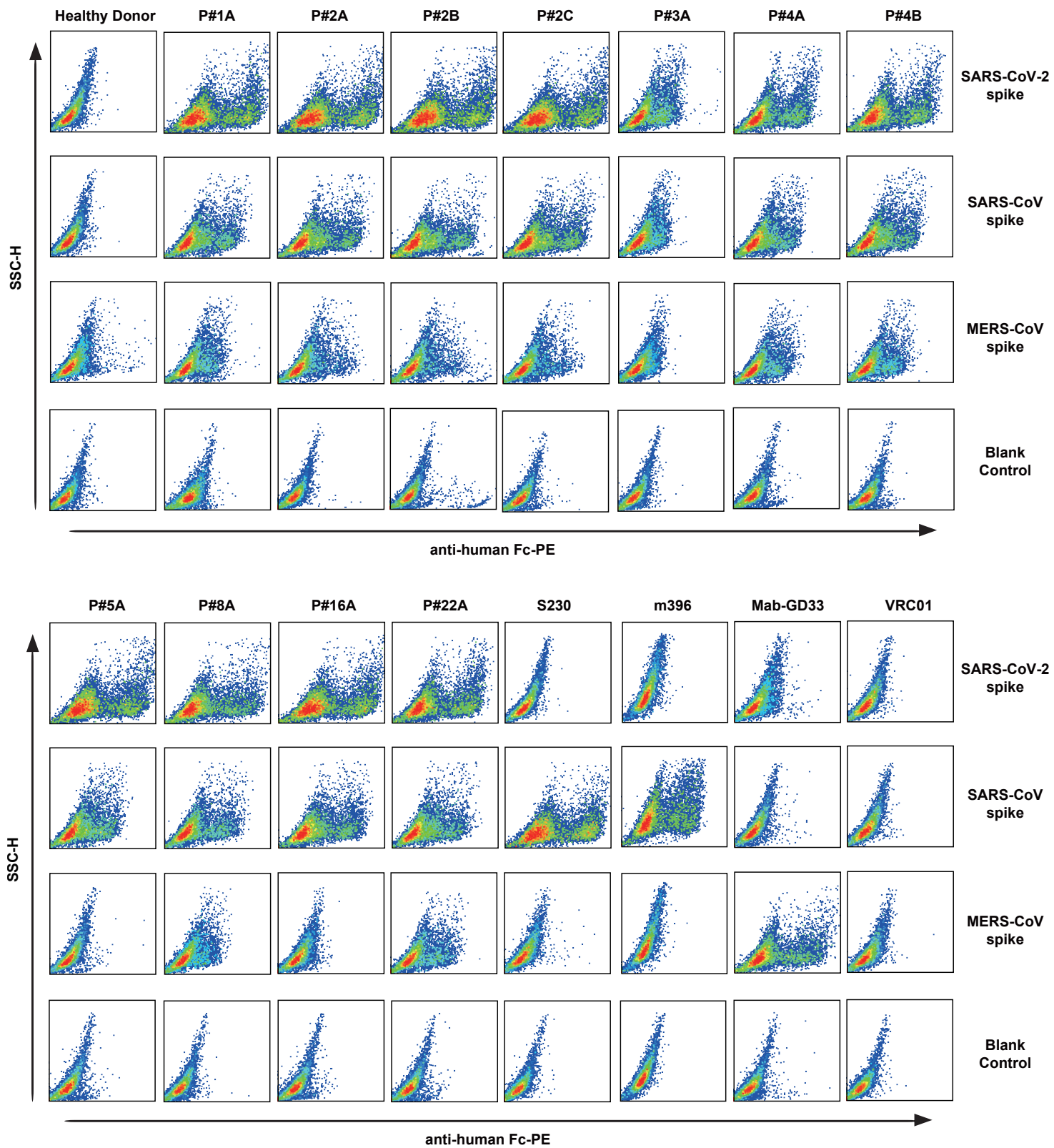
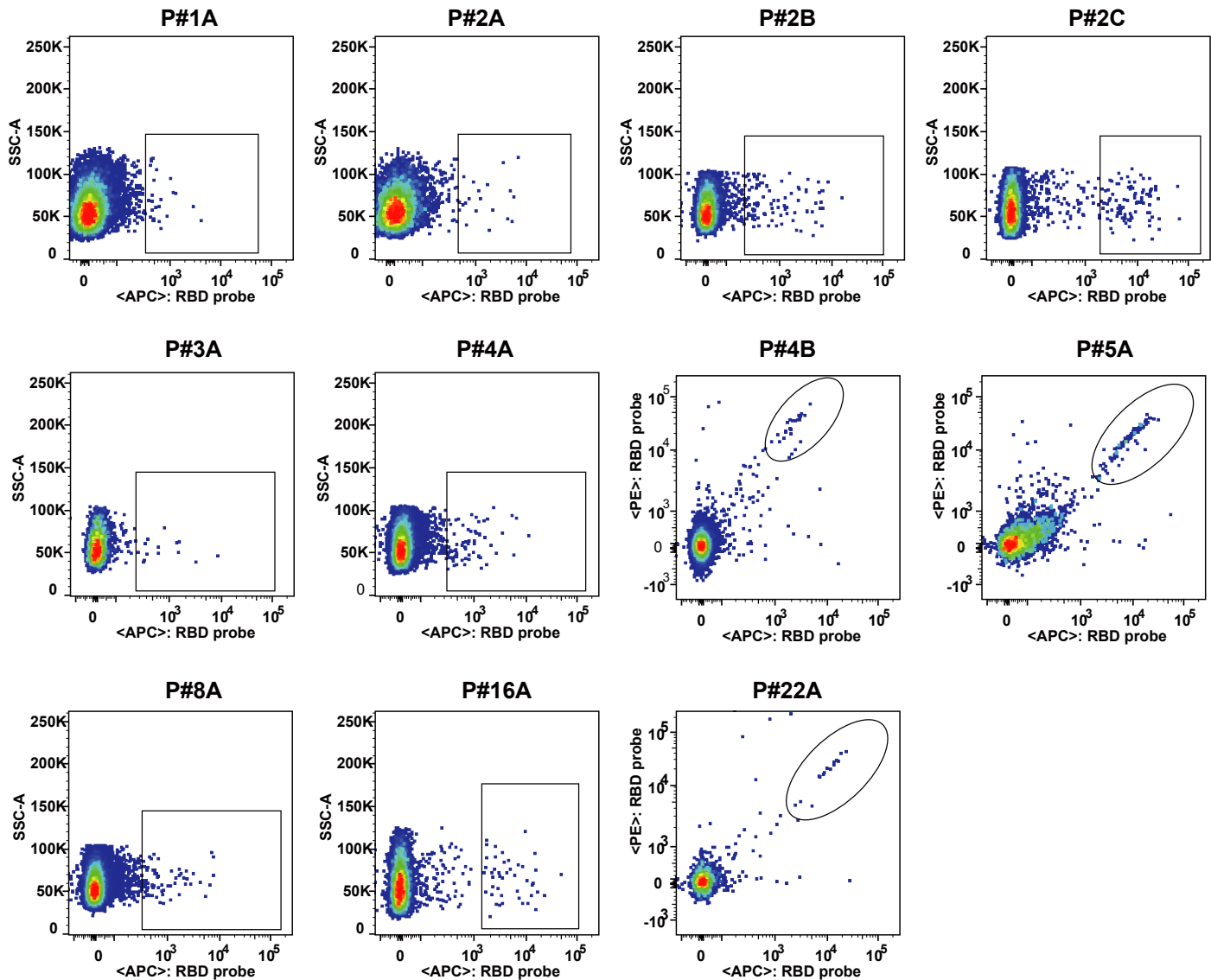


Figure S2



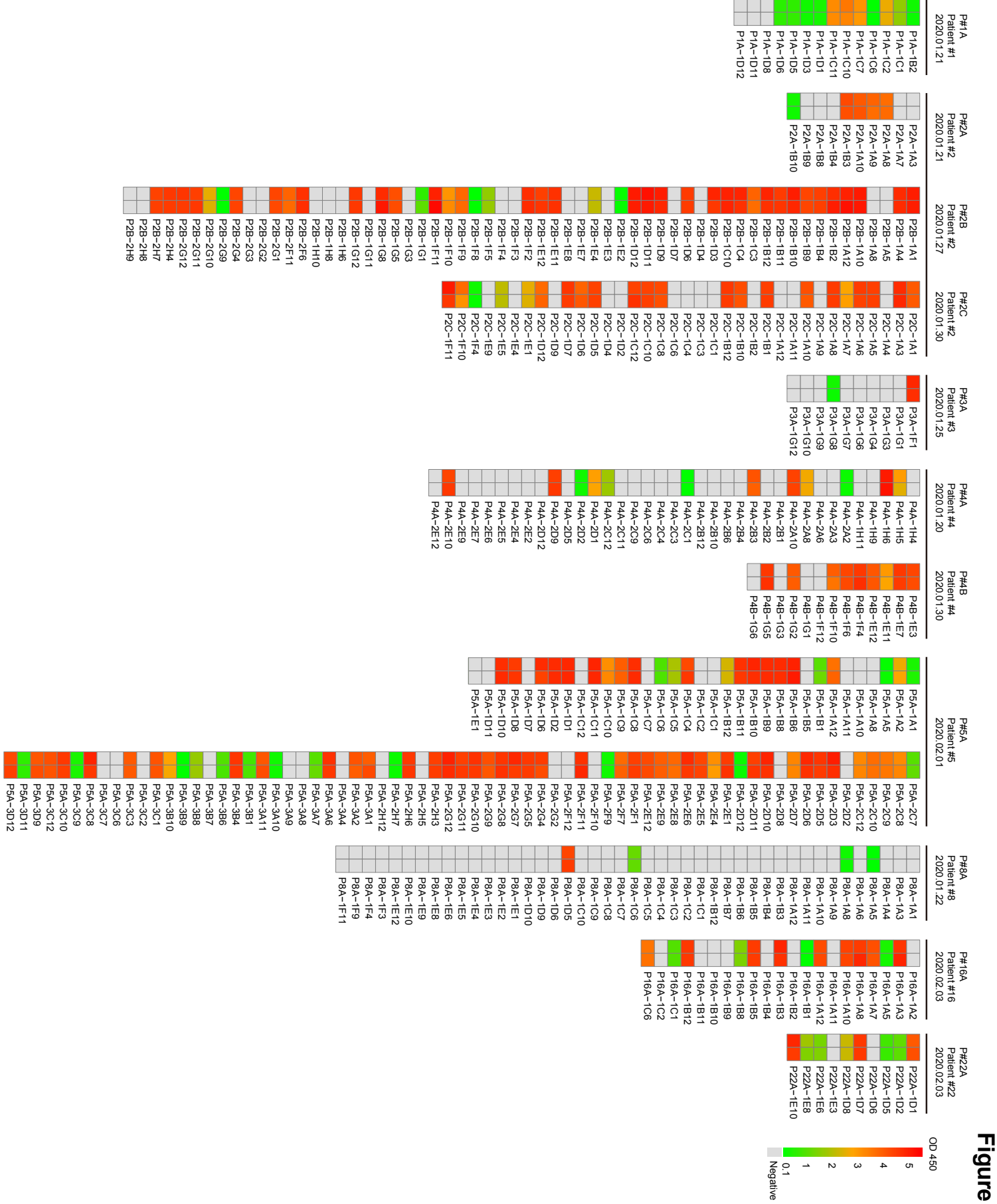
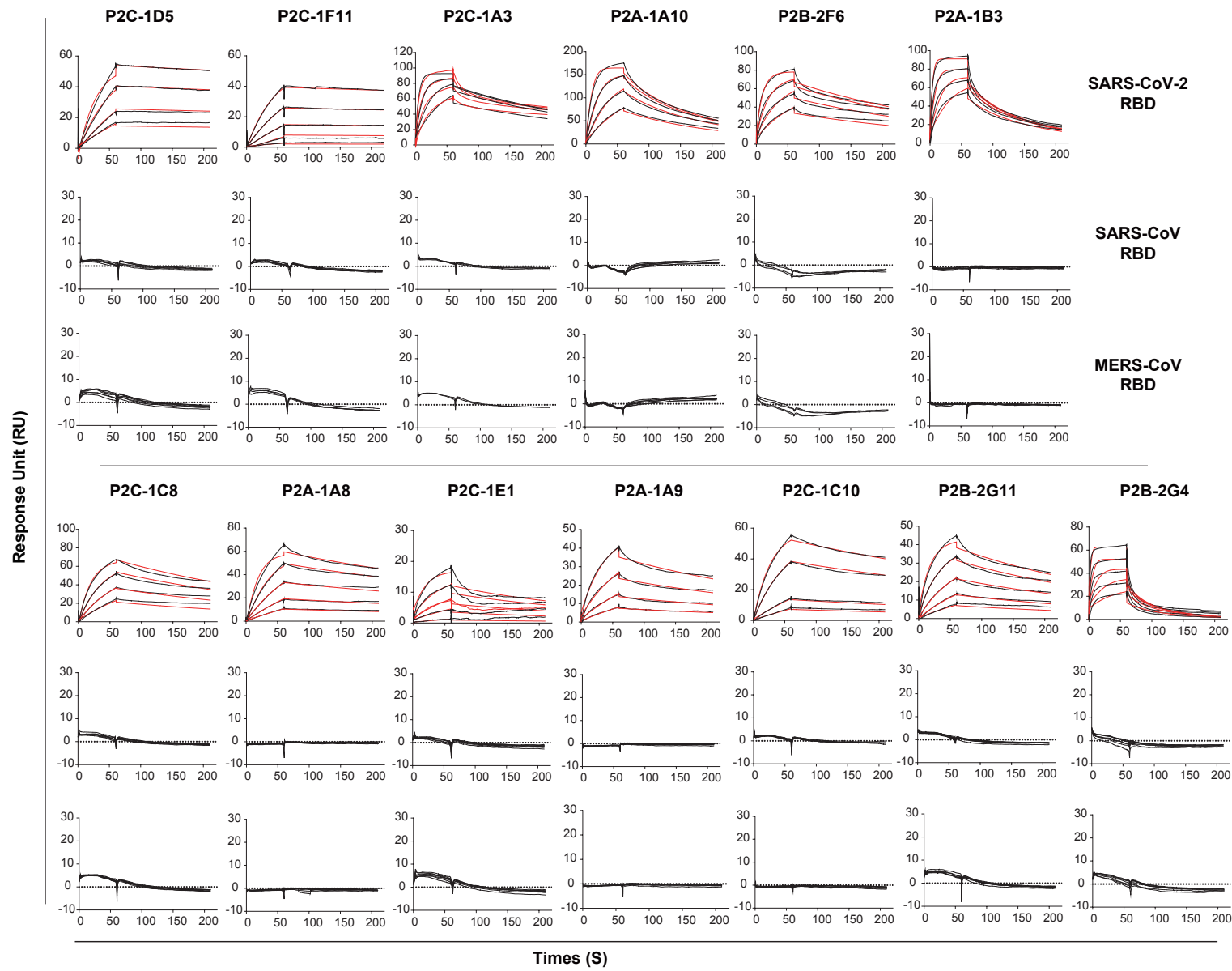


Figure S3

Figure S4

Patient #2



Patient #1

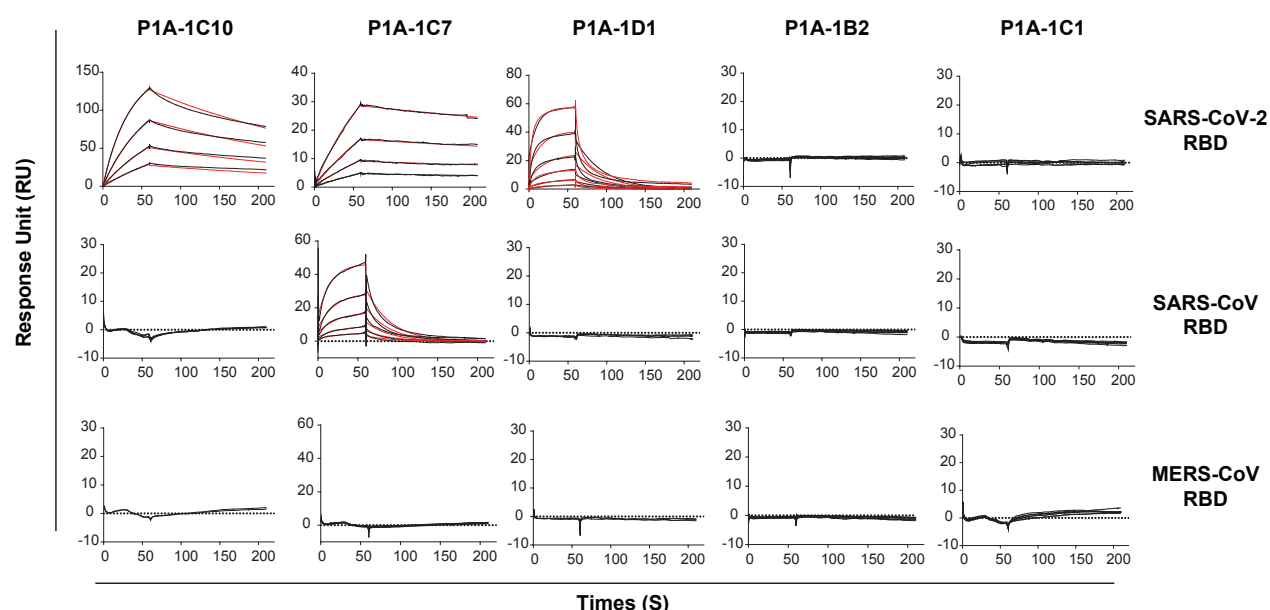
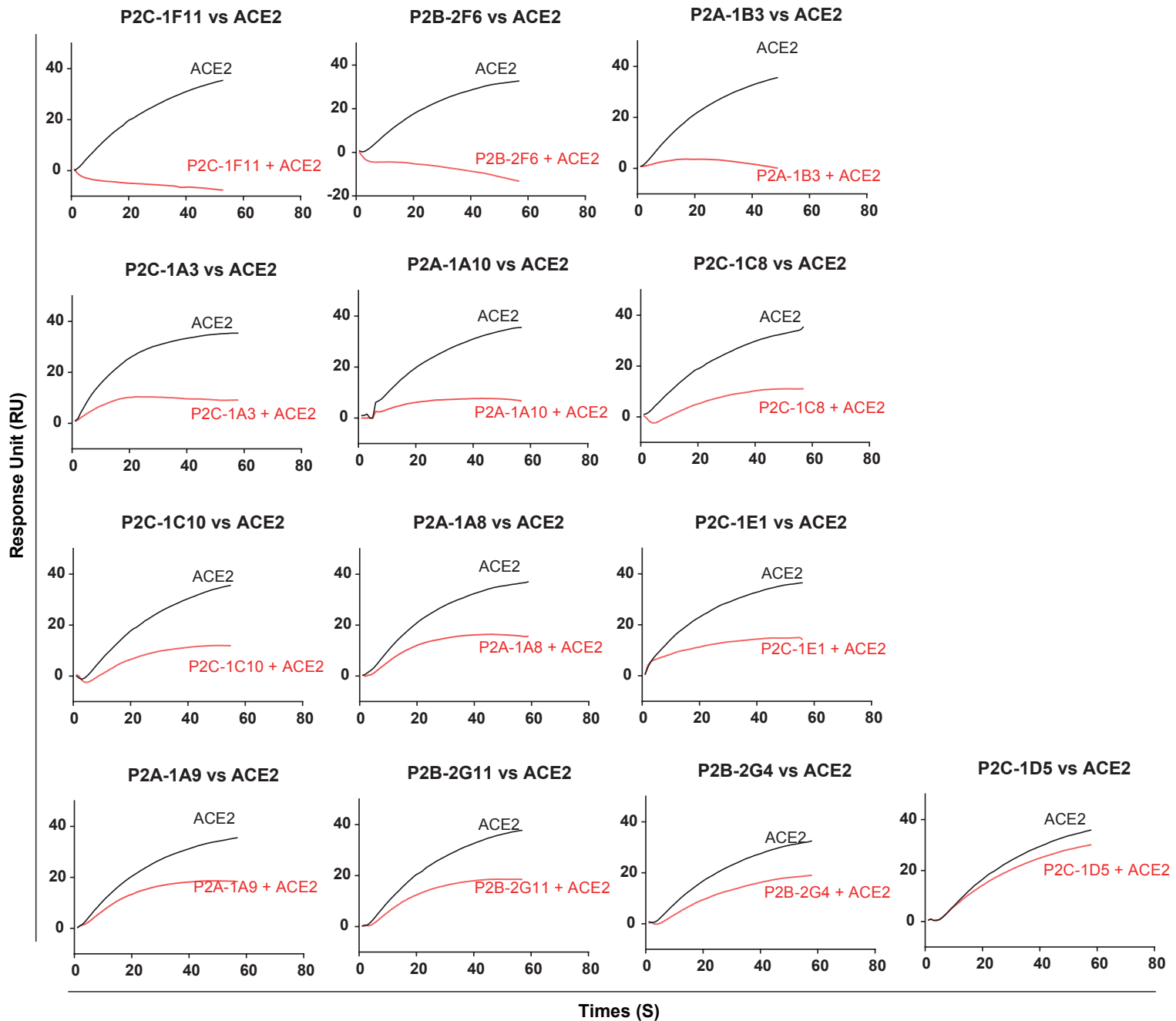


Figure S5

Patient #2



Patient #1

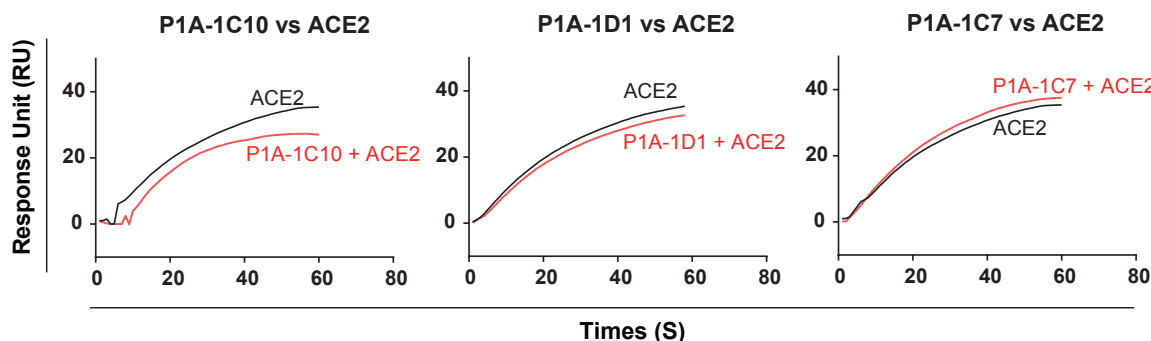


Figure S6

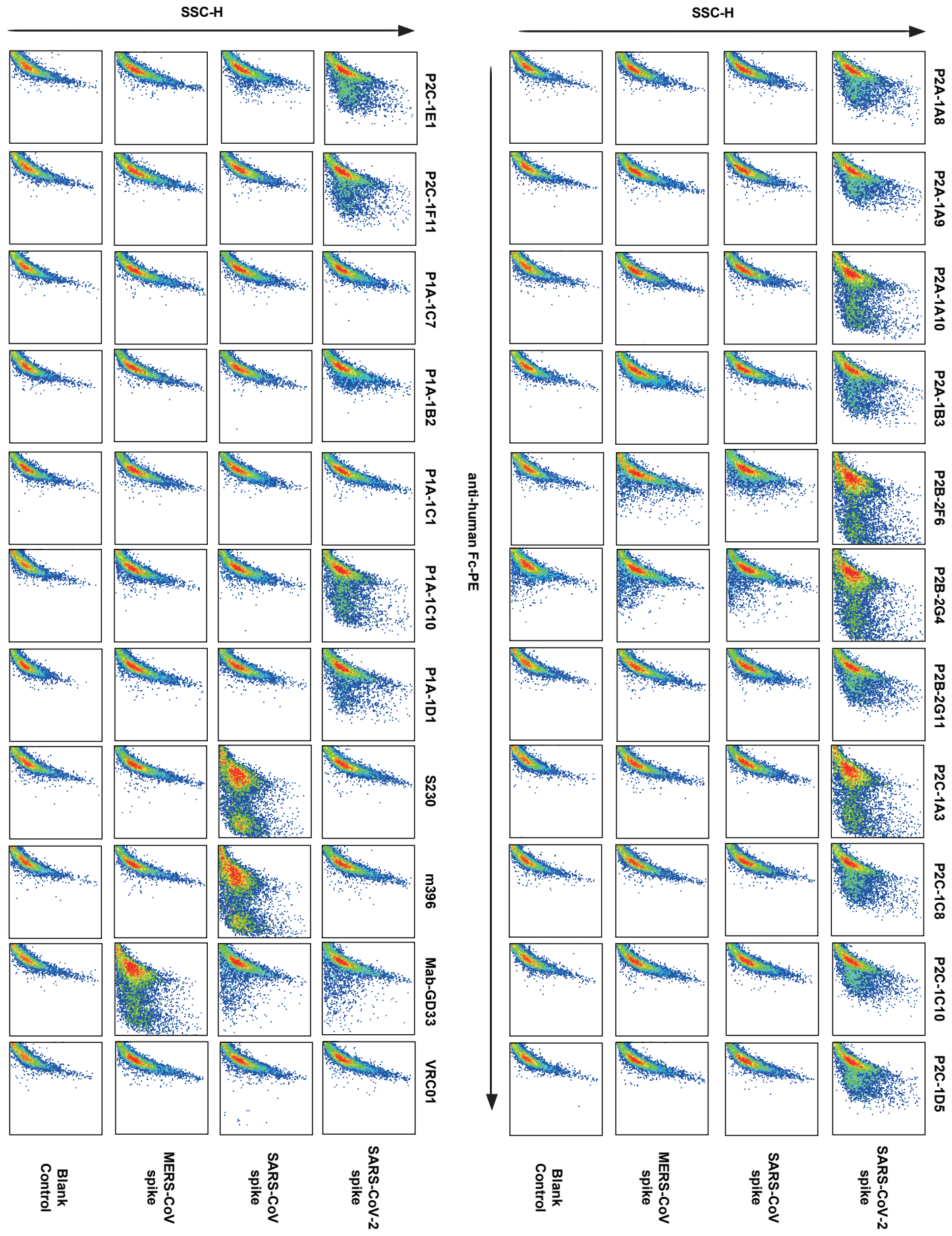


Figure S7

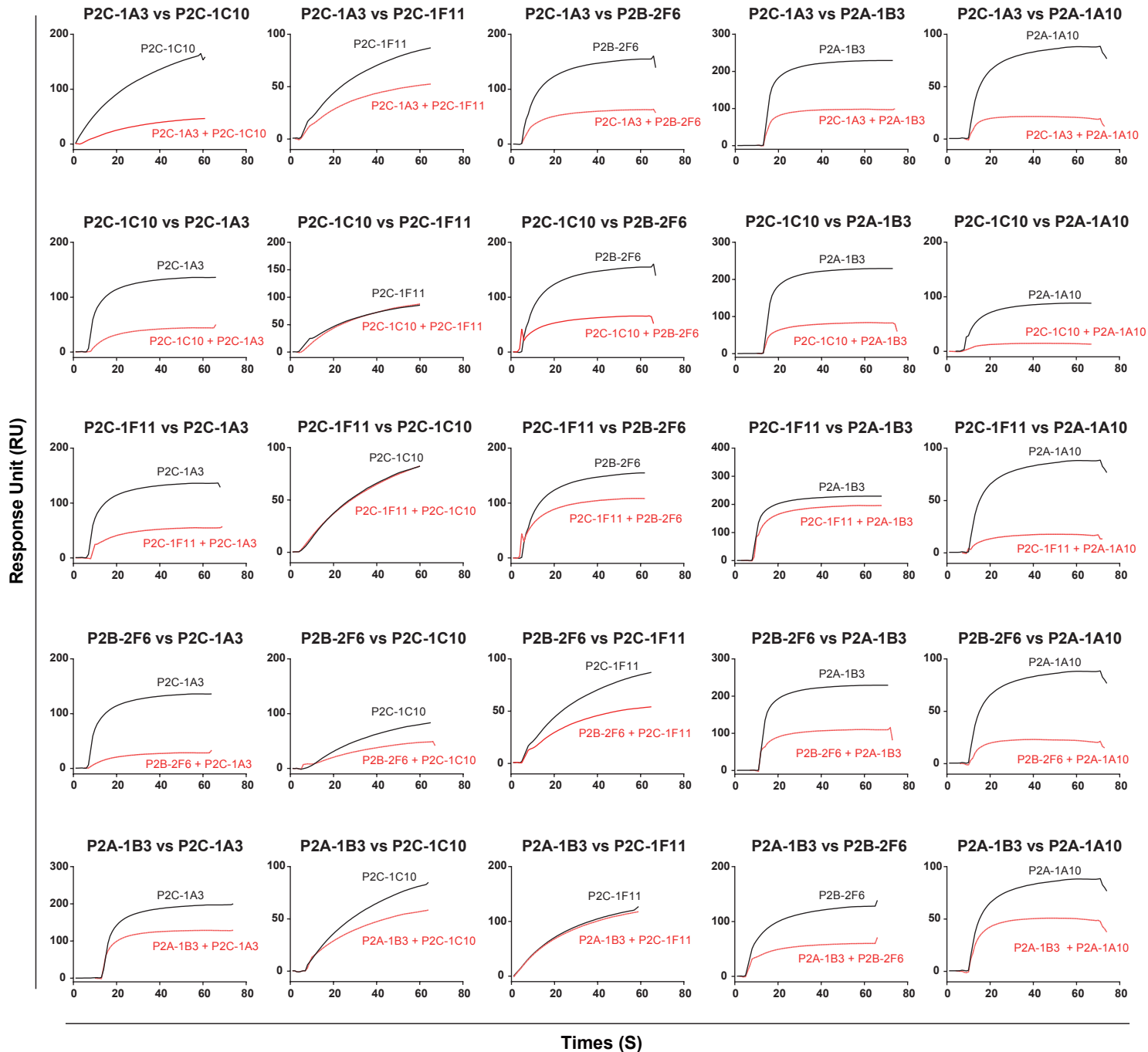


Table S1 Clinical characterization of the study subjects

Table S2. Gene family analysis of monoclonal antibodies.

Patient mAbs	Heavy chain				Kappa chain (KC) or Lambda chain (LC)					
	IGHV	IGHJ	IGHD	CDR3 length	SHM (%)	IGK(L)V	IGK(L)J	KC or LC	CDR3 length	SHM (%)
P#1 P1A-1C7	1-46*01,1-46*03	4*02	2-2*01	15	0.00	1-39*01,1D-39*01	3*01	KC	10	0.00
P#1 P1A-1C10	1-69*09	4*02	3-3*01	16	10.42	1-5*03	3*01	KC	9	3.41
P#1 P1A-1C11	1-69*09	4*02	3-3*01	16	10.42	1-5*03	3*01	KC	9	3.41
P#1 P1A-1C6	3-13*01	2*01	4-23*01	19	0.35	1-39*01,1D-39*01	3*01	KC	10	0.00
P#1 P1A-1D3	3-13*01	3*02	3-10*01	18	0.00	1-39*01,1D-39*01	1*01	KC	10	0.00
P#1 P1A-1C2	3-23*03	5*02	1-26*01	10	0.00	1-36*01	3*02	LC	11	0.00
P#1 P1A-1B2	3-30*03,3-30*18,3-30*5*01	4*02	5-24*01	12	11.46	2-14*01	2*01,3*01	LC	10	9.26
P#1 P1A-1C1	3-33*01,3-33*05,3-33*06	4*02	3-10*01	17	6.25	1D-13*01	5*01	KC	9	5.68
P#1 P1A-1D1	3-53*01	4*02	6-13*01	12	4.21	2-8*01	1*01	LC	10	2.22
P#1 P1A-1D5	3-53*01	6*02	2-15*01	15	1.05	1-33*01,1D-33*01	3*01	KC	9	0.00
P#1 P1A-1D6	3-53*01	6*02	2-15*01	15	4.56	1-33*01,1D-33*01	3*01	KC	9	3.79
P#2 P2A-1A10	1-2*06	2*01	2-2*01	19	0.00	2-40*01,2D-40*01	4*01	KC	9	0.00
P#2 P2B-1A4	1-2*06	2*01	2-2*01	19	0.00	2-40*01,2D-40*01	4*01	KC	9	0.00
P#2 P2B-1B2	1-2*06	2*01	2-2*01	19	0.00	2-40*01,2D-40*01	4*01	KC	9	0.00
P#2 P2B-2G1	1-2*06	2*01	2-2*01	19	0.00	2-40*01,2D-40*01	4*01	KC	9	0.00
P#2 P2B-2G12	1-2*06	2*01	2-2*01	19	0.00	2-40*01,2D-40*01	4*01	KC	9	0.00
P#2 P2C-1A10	1-2*06	2*01	2-2*01	19	0.00	2-40*01,2D-40*01	4*01	KC	9	0.00
P#2 P2C-1B10	1-2*06	2*01	2-2*01	19	0.00	2-40*01,2D-40*01	4*01	KC	9	0.00
P#2 P2C-1D6	1-2*06	2*01	2-2*01	19	0.00	2-40*01,2D-40*01	4*01	KC	9	0.00
P#2 P2C-1D12	1-2*06	2*01	2-2*01	19	0.00	2-40*01,2D-40*01	4*01	KC	9	0.00
P#2 P2C-1F10	1-2*06	2*01	2-2*01	19	0.00	2-40*01,2D-40*01	4*01	KC	9	0.00
P#2 P2B-1F8	1-2*06	6*02	3-4*01	14	8.33	3-20*01	1*01	KC	9	4.49
P#2 P2B-2G9	1-2*06	6*02	3-9*01	14	8.33	3-20*01	1*01	KC	9	4.49
P#2 P2B-1C3	1-46*01,1-46*03	3*01	2-2*01	15	0.00	1-5*03	1*01	KC	8	0.38
P#2 P2C-1C10	1-69*01,1-69*D01	4*02	4-23*01	11	0.35	3-11*01	2*01,2*02	KC	8	0.00
P#2 P2B-2G10	1-69*04	4*02	1-26*01	11	3.47	1-39*01,1D-39*01	2*01	KC	9	2.27
P#2 P2B-1F11	1-69*09	5*02	6-13*01	17	0.00	1-40*01	3*02	LC	11	0.00
P#2 P2B-1D9	2-5*02	4*02	3-10*01	16	1.03	1-47*02	2*01,3*01	LC	11	0.00
P#2 P2B-1E2	2-5*02	4*02	6-13*01	12	0.34	1-5*03	3*01	KC	8	0.00
P#2 P2B-1E4	2-5*02	4*02	5-12*01	11	0.00	2-14*01	2*01,3*01	LC	9	0.74
P#2 P2C-1F4	2-70*15	4*02	1-26*01	14	0.00	1-44*01	2*01,3*01	LC	10	0.00
P#2 P2B-1D12	3-11*04	5*01,5*02	6-13*01	12	0.00	1-9*01	4*01	KC	9	0.00
P#2 P2C-1A3	3-11*04	5*01,5*02	6-13*01	12	0.00	1-9*01	4*01	KC	9	0.00
P#2 P2B-1D6	3-15*01	6*02	3-10*01	24	0.00	1-44*01	3*02	LC	11	0.00
P#2 P2C-1B12	3-15*01	6*02	3-10*01	13	1.02	6-57*02	1*01	LC	10	0.00
P#2 P2B-1F9	3-15*01	4*02	3-22*01	16	0.00	1-NL1*01	1*01	KC	10	0.00
P#2 P2C-1D5	3-23*04	4*02	3-10*01	14	0.69	3-21*01	1*01	LC	11	0.38
P#2 P2B-1B4	3-30*04,3-30-3*03	6*02	3-10*01	22	0.35	1-39*01,1D-39*01	3*01	KC	10	0.00
P#2 P2B-1F2	3-33*01,3-33*06	4*02	5-18*01	11	0.00	2-11*01	2*01,3*01	LC	11	0.00
P#2 P2B-2G4	3-33*01,3-33*06	4*02	5-18*01	11	0.00	2-11*01	2*01,3*01	LC	11	0.00
P#2 P2C-1C8	3-33*01,3-33*06	4*02	3-22*01	13	0.69	2D-30*01	2*01	KC	9	0.36
P#2 P2A-1B3	3-48*02	5*02	3-10*01	16	10.07	3-20*01	5*01	KC	10	3.00
P#2 P2B-1B11	3-48*02	5*02	3-10*01	16	10.07	3-20*01	5*01	KC	10	2.62
P#2 P2B-1B12	3-48*02	5*02	3-10*01	16	10.07	3-20*01	5*01	KC	10	2.62
P#2 P2B-1C4	3-48*02	5*02	3-10*01	16	10.07	3-20*01	5*01	KC	10	3.00
P#2 P2B-1E11	3-48*02	5*02	3-10*01	16	10.07	3-20*01	5*01	KC	10	3.00
P#2 P2B-2H7	3-48*02	5*02	3-10*01	16	10.07	3-20*01	5*01	KC	10	2.62
P#2 P2B-1G12	3-48*02	5*02	3-10*01	16	8.33	3-20*01	5*01	KC	10	3.00
P#2 P2C-1E5	3-48*02	5*02	3-10*01	16	8.33	3-20*01	5*01	KC	10	3.00
P#2 P2B-1A10	3-53*01	3*02	1-20*01	15	0.35	1-33*01,1D-33*01	2*01	KC	10	0.38
P#2 P2B-1F5	3-53*01	4*02	2-2*01	14	0.00	1-NL1*01	1*01	KC	9	0.00
P#2 P2C-1D7	3-53*01	4*02	1-26*01	12	0.00	2D-30*01	3*01	KC	9	0.00
P#2 P2B-1G1	3-66*01,3-66*04	5*02	4-17*01	11	0.00	3-20*01	2*02	KC	9	0.00
P#2 P2C-1E1	3-66*01,3-66*04	4*02	5-12*01	9	0.00	3-11*01	1*01	KC	10	0.00
P#2 P2C-1F11	3-66*01,3-66*04	6*02	2-15*01	11	1.75	3-20*01	2*01,2*02	KC	8	0.00
P#2 P2A-1A8	3-9*01	6*02	5-12*01	23	3.82	2-14*02	1*01	LC	10	2.59
P#2 P2B-1B10	3-9*01	6*02	5-12*01	23	3.82	2-14*02	1*01	LC	10	2.59
P#2 P2B-1C10	3-9*01	6*02	5-12*01	23	3.82	2-14*02	1*01	LC	10	2.59
P#2 P2B-1D3	3-9*01	6*02	5-12*01	23	3.82	2-14*02	1*01	LC	10	2.59
P#2 P2B-2H4	3-9*01	6*02	5-12*01	23	3.82	2-14*02	1*01	LC	10	2.59
P#2 P2C-1A5	3-9*01	6*02	5-12*01	23	3.82	2-14*02	1*01	LC	10	2.59
P#2 P2C-1A8	3-9*01	6*02	5-12*01	23	3.82	2-14*02	1*01	LC	10	2.59
P#2 P2C-1B1	3-9*01	6*02	5-12*01	23	3.82	2-14*02	1*01	LC	10	2.59
P#2 P2C-1C12	3-9*01	6*02	5-12*01	23	3.82	2-14*02	1*01	LC	10	2.59
P#2 P2C-1A6	3-9*01	6*02	5-12*01	23	3.47	2-14*02	1*01	LC	10	2.59
P#2 P2A-1A9	3-9*01	6*02	3-22*01	17	2.08	1-40*01	2*01,3*01	LC	11	1.11
P#2 P2C-1A1	3-9*01	6*02	3-22*01	17	2.08	1-40*01	2*01,3*01	LC	11	1.11
P#2 P2B-2G11	3-9*01	6*02	1-26*01	17	2.08	1-40*01	2*01,3*01	LC	11	1.11
P#2 P2B-1E12	3-9*01	3*02	6-19*01	17	0.00	3-20*01	4*01	KC	9	0.00
P#2 P2B-2F6	4-38*2*02	3*02	2-2*01	20	0.69	2-8*01	3*02	LC	10	0.00
P#2 P2A-1B10	4-39*01	3*02	2-15*01	20	0.34	1-47*01	3*02	LC	8	0.37
P#2 P2B-1B9	4-39*07	4*02	4-17*01	9	0.00	1-NL1*01	1*01	KC	10	0.00
P#2 P2B-2F11	4-39*07	4*02	4-17*01	9	0.00	1-NL1*01	1*01	KC	10	0.00
P#2 P2B-1G8	4-39*07	4*02	5-12*01	11	0.34	1-5*03	3*01	KC	9	1.14
P#2 P2B-1A1	4-59*01	3*02	1-1*01	14	0.35	2-14*01	3*02	LC	10	1.11
P#2 P2B-1D11	4-59*01	5*02	2-15*01	22	0.00	3-25*03	2*01,3*01	LC	9	0.00

P#2	P2B-1F10	4-59*01,4-59*02	4*02	3-10*01	15	1.05	1-39*01,1D-39*01	2*01	KC	9	1.14
P#2	P2C-1A7	5-51*01	4*02	3-10*01	17	0.00	3-1*01	2*01,3*01,3*02	LC	9	0.00
P#2	P2B-1A12	7-4-1*02	6*02	5-12*01	16	0.00	1-39*01,1D-39*01	4*01	KC	9	0.00
P#2	P2B-1G5	7-4-1*02	6*02	4-23*01	12	1.04	3-21*01	3*02	LC	11	0.38
P#3	P3A-1F1	3-13*04	4*02	6-19*01	17	0.00	1-39*01,1D-39*01	1*01	KC	10	0.00
P#3	P3A-1G8	3-64*05,3-64D*06	6*02	3-10*01	19	0.35	1-44*01	2*01,3*01	LC	11	0.00
P#4	P4A-2A10	1-46*01,1-46*03	6*02	2-15*01	26	7.64	1-40*01	2*01,3*01	LC	10	1.85
P#4	P4B-1F6	1-69*01,1-69D*01	1*01	1-26*01	15	3.47	2-23*02	1*01	LC	10	1.85
P#4	P4B-1E11	2-5*02	4*02	3-10*01	18	0.00	1-36*01	3*02	LC	11	0.37
P#4	P4A-2A2	3-23*04	4*02	3-10*01	14	5.90	1-51*01	3*02	LC	11	2.25
P#4	P4A-2A8	3-23*04	4*02	4-11*01	11	0.00	3-21*01	2*01,3*01	LC	11	0.00
P#4	P4A-2C1	3-23*04	6*02	6-19*01	16	2.78	2-28*01,2D-28*01	4*01	KC	11	1.08
P#4	P4A-1H5	3-30*03,3-30*18,3-30-5*01	4*02	2-2*01	21	1.74	1-39*01,1D-39*01	3*01	KC	8	3.79
P#4	P4B-1G2	3-30*03,3-30*18,3-30-5*01	4*02	2-2*01	21	1.74	1-39*01,1D-39*01	3*01	KC	8	3.79
P#4	P4A-2B3	3-30*03,3-30*18,3-30-5*01	4*02	2-2*01	21	1.39	1-39*01,1D-39*01	3*01	KC	8	3.41
P#4	P4A-1H6	3-30*03,3-30*18,3-30-5*01	4*02	2-2*01	21	1.39	1-39*01,1D-39*01	3*01	KC	8	1.52
P#4	P4B-1G5	3-30*03,3-30*18,3-30-5*01	4*02	2-15*01	22	1.39	3-21*01	1*01	LC	10	0.77
P#4	P4A-2E10	3-30*03,3-30*18,3-30-5*01	4*02	2-2*01	21	4.86	1-39*01,1D-39*01	3*01	KC	8	1.89
P#4	P4B-1E3	3-30*03,3-30*18,3-30-5*01	4*02	2-2*01	21	4.86	1-39*01,1D-39*01	3*01	KC	8	1.89
P#4	P4A-2D9	3-30*03,3-30*18,3-30-5*01	4*02	2-2*01	21	2.08	1-39*01,1D-39*01	3*01	KC	8	2.27
P#4	P4B-1F4	3-30*,3-30*18,3-30-5*01	6*02	6-13*01	22	0.35	2-30*01	2*01	KC	10	0.00
P#4	P4B-1E7	3-43D*03	6*02	4-11*01	20	0.00	3-1*01	1*01	LC	10	0.00
P#4	P4B-1F10	3-7*01	6*02	3-*01	13	0.00	3-21*01	1*01	LC	12	0.00
P#4	P4A-2D1	3-9*01	4*02	4-23*01	13	0.00	1-12*01,1-12*02,1D-12*02	4*01	KC	9	0.00
P#4	P4A-2D2	4-39*01	6*02	3-22*01	16	0.00	3-20*01	4*01	KC	10	0.00
P#4	P4B-1E12	4-59*08	4*02	2-21*01	11	1.40	1-44*01	2*01,3*01	LC	11	0.37
P#4	P4A-2C12	5-51*01	4*02	3-22*01	15	2.43	1-44*01	1*01	LC	11	1.50
P#8	P8A-1A8	3-23*04	4*02	5-12*01	11	0.35	3-21*01	3*02	LC	11	0.77
P#8	P8A-1C6	3-30*03,3-30*18,3-30-5*01	4*02	2-15*01	20	0.00	1-33*01,1D-33*01	3*01	KC	8	0.00
P#8	P8A-1A5	5-51*01	6*03	5-18*01	18	1.74	1-47*02	1*01	LC	12	0.00
P#8	P8A-1D5	6-1*01	3*02	3-10*01	16	1.01	3-20*01	4*01	KC	9	0.37
P#5	P5A-1A1	1-24*01	5*02	3-10*01	15	0.35	2-28*01,2D-28*01	4*02	KC	9	0.00
P#5	P5A-1C8	1-46*01,1-46*03	1*01	3-22*01	22	0.00	1-33*01,1D-33*01	5*01	KC	10	0.00
P#5	P5A-2D5	1-46*01,1-46*03	3*02	3-*01	24	0.00	1-40*01	2*01,3*01	LC	11	0.00
P#5	P5A-2C8	1-46*01,1-46*03	4*02	5-12*01	15	0.00	2-23*02	1*01	LC	10	0.00
P#5	P5A-2E9	1-46*01,1-46*03	4*02	4-17*01	22	0.00	2-14*01	1*01	LC	11	0.74
P#5	P5A-3B8	1-46*01,1-46*03	4*02	3-10*01	16	0.69	2-23*02	7*01	LC	11	0.37
P#5	P5A-3A11	1-69*01,1-69D*01	6*02	2-15*01	14	0.00	1-39*01,1D-39*01	1*01	KC	9	0.00
P#5	P5A-3C10	1-69*01,1-69D*01	5*02	2-15*01	22	0.00	6-57*02	2*01,3*01	LC	8	0.00
P#5	P5A-1A2	1-8*01	5*02	3-3*01	21	0.69	1-40*01	1*01	LC	12	0.00
P#5	P5A-1C11	1-8*01	5*02	3-10*01	17	0.00	3-21*01	2*01,3*01	LC	13	0.38
P#5	P5A-2F11	1-8*01	5*02	2-2*01	15	0.00	4-1*01	4*01	KC	9	0.00
P#5	P5A-3B9	1-8*01	5*02	2-15*01	15	0.00	1-36*01	3*02	LC	11	0.00
P#5	P5A-2C12	2-5*02	4*02	6-13*01	16	0.00	3-11*01	4*01	KC	8	0.00
P#5	P5A-3C12	2-5*02	4*02	6-13*01	19	0.00	4-1*01	2*01	KC	9	0.00
P#5	P5A-3C3	2-5*02	4*02	2-15*01	12	0.34	6-57*02	2*01,3*01	LC	9	0.00
P#5	P5A-3C1	3-11*01	5*02	6-13*01	13	1.39	3-21*01	2*01	LC	13	0.00
P#5	P5A-1C4	3-13*01	6*02	3-10*01	20	0.00	1-39*01,1D-39*01	2*01	KC	10	0.00
P#5	P5A-2G8	3-13*01	4*02	1-26*01	13	0.70	1-39*01,1D-39*01	3*01	KC	10	0.00
P#5	P5A-2D3	3-13*01	2*01	6-13*01	16	0.00	1-39*01,1D-39*01	5*01	KC	10	0.00
P#5	P5A-3B10	3-13*01	2*01	6-13*01	16	0.00	1-39*01,1D-39*01	3*01	KC	10	0.00
P#5	P5A-1D8	3-15*01	3*02	3-22*01	18	0.68	3-19*01	2*01,3*01	LC	11	0.00
P#5	P5A-2G10	3-15*01	3*02	3-22*01	18	0.00	3-19*01	2*01,3*01	LC	11	0.00
P#5	P5A-2H6	3-15*01	3*02	3-22*01	18	0.00	3-19*01	2*01,3*01	LC	11	0.00
P#5	P5A-1D6	3-23*04	4*02	1-1*01	13	0.00	3-21*01	3*02	LC	11	0.00
P#5	P5A-2E12	3-23*04	4*02	6-19*01	14	0.00	3-21*01	1*01	LC	11	0.00
P#5	P5A-3D12	3-23*04	3*02	3-22*01	24	0.35	1-47*01	1*01	LC	12	0.00
P#5	P5A-1B6	3-30*04,3-30-3*03	4*02	3-10*01	20	0.00	1-33*01,1D-33*01	2*01	KC	9	0.00
P#5	P5A-2E6	3-30*04,3-30-3*03	4*02	3-10*01	20	0.00	1-33*01,1D-33*01	2*01	KC	9	0.00
P#5	P5A-1B1	3-33*01,3-33*04,3-33*06	4*02	4-23*01	14	3.13	3-15*01	4*01	KC	9	1.89
P#5	P5A-1C5	3-33*01,3-33*04,3-33*06	4*02	4-23*01	14	3.13	3-15*01	4*01	KC	9	2.27
P#5	P5A-2H7	3-33*01,3-33*04,3-33*06	4*02	4-23*01	14	3.13	3-15*01	4*01	KC	9	1.89
P#5	P5A-2G9	3-33*01,3-33*06	4*02	3-10*01	12	0.00	5-37*01	1*01	LC	10	0.35
P#5	P5A-2G11	3-33*01,3-33*06	6*02	3-16*01	17	0.00	2-14*01	2*01,3*01	LC	11	0.74
P#5	P5A-1B8	3-53*01	4*02	2-15*01	9	1.40	1-9*01	4*01	KC	9	0.00
P#5	P5A-1D2	3-53*01	4*02	1-26*01	15	1.40	1-40*01	2*01,3*01	LC	11	1.11
P#5	P5A-1D1	3-53*01	6*02	3-16*01	11	0.35	1-9*01	5*01	KC	8	0.76
P#5	P5A-2C9	3-7*01	4*02	6-19*01	14	0.00	3-20*01	5*01	KC	10	0.00
P#5	P5A-2E4	3-7*01	4*02	6-19*01	14	0.35	3-20*01	5*01	KC	10	0.00
P#5	P5A-2G12	3-7*01	4*02	5-18*01	12	0.00	6-57*02	2*01,3*01	LC	10	0.00
P#5	P5A-2D12	3-7*01	6*02	4-11*01	18	0.00	2-28*01,2D-28*01	1*01	KC	9	0.00
P#5	P5A-2F1	3-74*02	4*02	6-19*01	12	0.00	6-57*02	2*01,3*01	LC	9	0.00
P#5	P5A-1C10	3-9*01	4*02	4-17*01	14	0.00	3-21*01	1*01	LC	12	0.00
P#5	P5A-2E8	3-9*01	4*02	4-17*01	13	0.00	3-21*01	1*01	LC	11	0.00
P#5	P5A-3A2	3-9*01	4*02	4-17*01	14	1.74	3-21*01	1*01	LC	11	0.00
P#5	P5A-2D6	3-9*01	4*02	3-10*01	14	0.35	1-40*01	2*01,3*01	LC	12	0.74
P#5	P5A-1B12	3-9*01	6*02	4-17*01	17	0.69	1-51*01	2*01,3*01	LC	11	0.37
P#5	P5A-3A6	3-9*01	6*02	3-10*01	27	0.69	2-14*01	2*01,3*01	LC	10	0.74
P#5	P5A-3D9	3-9*01	3*02	3-3*02	16	0.00	3-15*01	4*01	KC	11	0.38

P#5	P5A-1D10	3-11*01	4*02	3-16*02	21	2.43	2-14*01	2*01,3*01	LC	11	1.11
P#5	P5A-3A1	3-53*01	4*02	4-17*01	11	0.00	3-20*01	2*02	KC	9	0.00
P#5	P5A-3C8	3-53*01	6*02	4-11*01	11	1.05	1-9*01	2*01	KC	11	1.14
P#5	P5A-2D10	4-31*03	5*02	5-12*01	12	0.34	6-57*02	2*01,3*01	LC	10	0.37
P#5	P5A-2G5	4-31*03	4*02	3-16*02	14	1.37	3-21*01	2*01,3*01	LC	11	0.00
P#5	P5A-1A12	4-39*01	6*02	2-21*01	17	0.69	4-1*01	1*01	KC	9	0.00
P#5	P5A-2C7	4-39*01	4*02	4-17*01	16	0.00	2-23*02	3*02	LC	10	0.00
P#5	P5A-2F7	4-39*01	4*02	3-22*01	18	0.00	2-23*02	1*01	LC	11	0.00
P#5	P5A-2F9	4-39*01	4*02	3-9*01	14	0.00	2-23*02	2*01,3*01	LC	8	0.00
P#5	P5A-1A5	4-4*02	4*02	4-23*01	14	0.00	2-14*01	2*01,3*01	LC	10	0.74
P#5	P5A-1C6	4-4*02	5*02	2-8*02	22	0.00	1-40*01	1*01	LC	12	0.00
P#5	P5A-3A10	4-4*02	6*02	6-13*01	21	0.00	1-39*01,1D-39*01	2*01	KC	9	0.00
P#5	P5A-1B9	4-59*01	2*01	3-9*01	22	0.70	4-1*01	4*01	KC	9	0.00
P#5	P5A-3A7	4-59*01	2*01	3-9*01	22	0.00	4-1*01	4*01	KC	9	0.00
P#5	P5A-3B1	4-59*01	2*01	3-9*01	22	0.00	4-1*01	4*01	KC	9	0.00
P#5	P5A-3B6	4-59*01	2*01	3-9*01	22	0.00	4-1*01	4*01	KC	9	0.00
P#5	P5A-2C10	4-59*01	1*01	4-17*01	17	0.00	3-21*01	2*01,3*01	LC	11	0.00
P#5	P5A-2E5	4-59*01	4*02	5-12*01	12	0.00	6-57*02	2*01,3*01	LC	9	0.00
P#5	P5A-2G4	4-59*12	3*02	2-8*02	12	10.88	1D-16*01	5*01	KC	9	2.65
P#5	P5A-2G7	4-61*01	5*02	3-10*01	20	0.34	2-14*01	2*01,3*01	LC	11	0.74
P#5	P5A-1B10	5-51*01	4*02	3-16*01	12	1.04	2-28*01,2D-28*01	2*01	KC	11	0.72
P#5	P5A-1C9	5-51*01	4*02	6-19*01	11	0.00	3-19*01	1*01	LC	12	0.00
P#5	P5A-2D11	5-51*01	4*02	4-23*01	13	0.00	1-44*01	2*01,3*01	LC	11	0.00
P#5	P5A-3B4	5-51*01	4*02	4-23*01	13	0.35	1-44*01	2*01,3*01	LC	11	0.00
P#5	P5A-2H3	5-51*01	4*02	4-23*01	13	0.35	1-44*01	2*01,3*01	LC	11	0.00
P#5	P5A-2E1	5-51*01	5*02	4-11*01	12	0.00	3-21*01	2*01,3*01	LC	11	0.00
P#5	P5A-1B11	7-4-1*02	4*02	2-15*01	20	0.00	1-39*01,1D-39*01	4*01	KC	10	0.00
P#5	P5A-2D7	7-4-1*02	6*02	6-19*01	10	0.00	6-21*02	1*01	KC	8	0.00
P#5	P5A-3C9	7-4-1*02	6*02	6-19*01	10	0.00	6-21*02	1*01	KC	8	0.00
P#5	P5A-3D11	7-4-1*02	6*02	6-19*01	10	0.00	6-21*02	1*01	KC	8	0.00
P#16	P16A-1A3	1-3*01	5*02	5-18*01	11	0.00	6-57*02	2*01,3*01	LC	9	0.37
P#16	P16A-1A8	1-46*01,1-46*03	4*02	2-2*01	20	0.00	3-21*01	1*01	LC	13	0.00
P#16	P16A-1B5	1-46*01,1-46*03	4*02	3-3*01	13	0.00	3-21*02	2*01,3*01	LC	12	0.00
P#16	P16A-1C6	1-46*01,1-46*03	1*01	6-19*01	16	0.69	3-21*02	3*02	LC	12	0.38
P#16	P16A-1C1	3-13*01	6*03	6-13*01	21	0.00	1-39*01,1D-39*01	1*01	KC	10	0.00
P#16	P16A-1A5	3-33*01,3-33*06	4*02	6-25*01	15	0.00	1-33*01,1D-33*01	4*01	KC	9	0.38
P#16	P16A-1A12	3-33*01,3-33*06	4*02	2-21*02	19	0.35	1-51*01	3*02	LC	11	0.75
P#16	P16A-1B1	3-74*02	5*02	6-13*01	15	2.43	1-36*01	2*01,3*01	LC	11	3.37
P#16	P16A-1B3	3-9*01	6*02	6-13*01	24	0.35	3-1*01	1*01	LC	10	0.00
P#16	P16A-1B12	4-34*01	6*03	2-2*01	16	0.00	1-51*01	2*01,3*01	LC	11	0.37
P#16	P16A-1B8	5-51*01	4*02	3-16*02	19	0.00	3-1*01	2*01,3*01	LC	11	0.00
P#16	P16A-1A7	7-4-1*02	3*02	1-26*01	14	0.69	3-21*01	2*01,3*01	LC	12	0.00
P#16	P16A-1A10	7-4-1*02	3*02	1-20*01	15	0.00	3-21*02	3*02	LC	12	0.00
P#22	P22A-1E10	1-46*01,1-46*03	6*02	2-2*01	15	0.00	3-11*01	3*01	KC	10	0.00
P#22	P22A-1D2	1-8*01	5*02	3-3*01	21	0.00	1-40*01	1*01	LC	12	0.00
P#22	P22A-1D8	3-23*04	4*02	3-22*01	20	10.42	3-15*01	1*01	KC	10	3.03
P#22	P22A-1D7	3-33*01,3-33*06	4*02	4-17*01	13	0.35	1-39*01,1D-39*01	1*01	KC	10	0.38
P#22	P22A-1D1	3-53*01	6*02	No results	11	0.00	1-9*01	1*01	KC	8	0.38
P#22	P22A-1E8	3-9*01	4*02	6-19*01	16	0.00	3-15*01	4*01	KC	11	0.00
P#22	P22A-1D5	4-39*01	4*02	5-24*01	14	0.00	2-23*01,2-23*03	1*01	LC	8	0.00
P#22	P22A-1E6	4-59*01	4*02	3-22*01	16	0.00	3-20*01	4*01	KC	9	0.37

The program IMGT/V-QUEST was applied to analyze gene germline, complementarity determining region (CDR) 3 length, and somatic hypermutation (SHM). The CDR3 length was calculated from amino acids sequences. The SHM frequency was calculated from the mutated nucleotides.